Front. Earth Sci. 2024, 18(1): 127−147
https://doi.org/10.1007/s11707-022-1050-x

RESEARCH ARTICLE

Combined effects of massive reclamation and dredging on the variations in hydrodynamic and sediment transport in Lingdingyang Estuary, China

Kanglin CHEN[1,2], Yitong LIN[3,4], Jing LIU[3,4], Zixiao HE[3,4], Liangwen JIA (✉)[3,4,5]

1 School of Geography and Remote Sensing, Guangzhou University, Guangzhou 510006, China
2 School of Marine Science, Sun Yat-Sen University, Guangzhou 510275, China
3 School of Marine Engineering and Technology, Sun Yat-Sen University, Guangzhou 510275, China
4 Southern Marine Science and Engineering, Guangdong Laboratory (Zhuhai), Zhuhai 519080, China
5 Guangdong Province Engineering Research Center of Coasts, Islands and Reefs, Guangzhou 510275, China

Abstract Anthropogenic disturbances associated with the rapid development of coastal cities have drastically influenced the hydrodynamics and sediment transport processes in many large estuaries globally. Lingdingyang Estuary (LE), located in the central and southern part of the Pearl River Delta, southern China with a long history of high-intensity anthropogenic disturbances, was studied to explore the contribution rate and mechanism underlying the alteration in hydrodynamics and sediment transport under each phase of human activity. A state-of-the-art modeling tool (TELEMAC-2D), was used to study the variations in the hydrodynamics and sediment transport, accounting for reclamation-induced shoreline and dredging-induced topography changes. The results indicated that: i) under the influence of successive land reclamation, the general distribution of the Confluence Hydrodynamic Zone (CHZ) in LE varied from scattered to concentrated, and these zones moved 3–5 km seaward. ii) Large-scale channel dredging weakened the residual flow in LE, decreasing the residual flow in the Inner-Lingding Estuary (ILE) by 62.45%. This was initiated by the enhancement of tidal dynamics through changes in the bottom friction caused by dredging in the ILE. In contrast, massive reclamation decreased the residual flow in the ILE by 17.55% and increased that in the Outer-Lingding Estuary (OLE). iii) Despite disturbances related to land reclamation and dredging, the estuarine jet flow in LE remained a turbulent jet system, and the estuarine jet flow became more asymmetrical. In addition, the position of the estuarine jet source moved 6–13 km seaward. iv) Both reclamation and dredging decreased the SSC in the ILE and increased the SSC in the OLE. Reclamation weakened the SSC in the ILE by 62.19%, whereas dredging enhanced the SSC in the OLE by 49%. Spatially, reclamation resulted in an increase in the SSC near the outlets and a decrease in the SSC in the northern portion of the Western Channel. Dredging mainly increased the SSC in the northern part of the OLE. v) The increase in the barotropic pressure gradient was the main factor driving the enhancement of the residual flow and SSC near the outlets. Moreover, the southward location of the "artificial outlets" favored the transport of suspended sediments to the OLE, which was one of the primary reasons for the increase in the SSC in the OLE. Finally, the tidal dynamics of the ILE intensified due to massive reclamation and dredging. The findings of this study indicate that hydrodynamics and sediment transport in LE have greatly changed over the last decades, with reclamation and dredging being the crucial drivers. The insights obtained from this study can serve as a reference for the comprehensive management of the Pearl River Estuary and other large estuaries experiencing similar anthropogenic forcing.

Keywords reclamation and dredging, estuarine jet flow, dynamics and sediment transport mechanism, Lingdingyang Estuary

1 Introduction

Estuaries form the interface between river systems and ocean systems (Pritchard, 1967; Li, 2004). Estuarine regions are among the most densely populated areas in the world and experience tremendous human activities.

Received November 10, 2022; accepted January 29, 2023

E-mail: jialwen@126.com

The abundant resources in these areas have become the targets of exploitation in various fields of study (Chen and Chen, 2002). Estuaries worldwide have been subjected to severe anthropogenic effects due to rapid urbanization and industrialization over the past decades (Anthony et al., 2015; Wang et al., 2015). Human intervention in the form of dam construction in the upstream reaches of rivers, extensive reclamation, large-scale navigation channel dredging, and sand mining can result in irreversible variations in estuarine dynamics and morphology, and can alter the natural evolution trend of estuaries (Dam et al., 2013; Winterwerp and Wang, 2013; Perkins et al., 2015; Zhu et al., 2016).

High-intensity reclamation is commonly practiced at large scales to accommodate economic growth in many estuaries globally (Maselli and Trincardi, 2013; Woodruff et al., 2013; Gao et al., 2014; Yang and Chui, 2017; Chu et al., 2022). For instance, because of the demand for urban land, the area of reclaimed land in Chongming North Shoal in the Yangtze Estuary has reached ~400 km^2 in recent decades; this has weakened the effect of runoff and enhanced the effect of tidal currents in the North Branch of the estuary, leading to the frequent occurrence of tidal bores and saltwater intrusion into its South Branch (Song, 2013). Shen et al. (2022) pointed out that reclamation projects significantly affected the residual current fields and decreased tidal prisms across the Pearl River Estuary, resulting in alterations in the water exchange and material transport process. Moreover, reclamation can increase tidal wave deformation (Gao et al., 2014), change plume and sediment transport (Choi, 2014), and increase estuarine turbidity (Winterwerp et al., 2013). van Maren et al. (2023) reported that reclaiming intertidal areas resulted in immediate loss of tidal storage, which led to amplification and faster propagation of tides. Maren et al. (2016) found that shoreline reclamation was an important factor influencing the significant increase in the suspended sediment concentration (SSC) in Ems Estuary at the Dutch German border. In addition, the bathymetry changes imposed by dredging not only directly modify the local geomorphology, but also lead to rapid variations in the estuarine hydrodynamics (Ralston et al., 2019). Massive dredging can alter the plume and sediment transport (Smith and Friedrichs, 2011; van Maren et al., 2015) as well as enhance tidal forcing and estuarine circulation (Winterwerp et al., 2013; Grasso and Le Hir, 2019). Reid et al. (2022) reported that the gradual process of channel deepening by dredging in the Santos channel in Brazil resulted in modified estuarine circulation parameters such as tidal propagation and water column stratification, leading to an increase in saline intrusion and a decrease in the volume of water transported through the channel. In large estuaries, various human activities may have important effects on the hydrodynamics and sediment transport processes (i.e., residual current, estuarine jet flow, and SSC). However, there is lack of quantitative studies on these effects and their consequences for the development of tidal flat resources and channel regulation.

Lingdingyang Estuary (LE) in the central and southern part of the Pearl River Delta, southern China, is one of the largest and most densely urbanized regions in the world. Between 1955 and 2010, ~200 km^2 of tidal flats in LE were reclaimed (Wu et al., 2016a), and large-scale navigation channel dredging was carried out primarily from 2000 to 2015 (Chen et al., 2020). These activities caused drastic changes in the estuarine boundary, such as the discernible seaward shift of the four eastern outlets and a significant change in the average bathymetric depth of the channels in LE from −7 m in the 1970s to −16 m in the 2010s (Li, 2017; Chen et al., 2020). Most previous studies have focused on the impacts of human activities on long-term morphological evolution in LE (Wu et al., 2016a). Chen et al. (2022) reported that the contribution rate of upstream sediment reduction to long-term geomorphic evolution was 61%, and that of reclamation was 16% for the whole LE during 1978–1998. However, changes in estuarine jet flow and sediment transport in large trumpet estuaries during flood seasons under anthropogenic forcing are still not well understood. Importantly, since LE has a long history of human activity with clear shoreline and bathymetry change records, it is a valuable target area that can provide insights on these aspects. Additionally, there is an urgent need to obtain a systematic understanding of the combined effects of massive reclamation and dredging on the variations in hydrodynamic and SSC in LE during flood seasons, as it is one of the most vulnerable estuaries to flooding worldwide (Hallegatte et al., 2013).

The primary objectives of this study were to 1) explore the response of estuarine dynamics and sediment transport in large trumpet estuaries such as LE to massive reclamation and dredging; 2) analyze the contribution of high-intensity reclamation and channel dredging to changes in the estuarine jet flow; 3) reveal the mechanism by which reclamation and dredging cause changes in the regimes of estuarine dynamics. In this study, a state-of-the-art numerical model (TELEMAC-MASCARET (TELEMAC-2D)) was employed to investigate the response of estuarine dynamics and sediment transport to land reclamation and dredging. To fully depict the process of estuarine hydrodynamics and sediment response, the model was composed of rivers, outlets, and estuarine bays. It was validated using tidal level, velocity, and SSC data obtained at multiple stations within the bay. Subsequently, a series of numerical experiments was designed to explore the response of i) residual currents, ii) estuarine jet flow, and iii) SSC to massive reclamation and dredging. Finally, the impacts of large-scale reclamation, dredging, and combined reclamation and dredging on hydrodynamics and SSC were quantified.

2 Regional setting

The LE, a funnel-shaped estuary-bay system in the central and southern part of the Pearl River Delta, south of China, covers an area of 1180 km^2. LE is approximately 60 km long with a narrow neck near the Humen outlet in the north and a wide mouth in the south. Historically, 50%–55% of the river runoff and ~45% of the sediment were discharged from the Pearl River via four eastern outlets, namely the Humen, Jiaomen, Hongqili, and Hengmen outlets. The Humen outlet is dominated by tides, with an average ratio between runoff discharge and tidal discharge of 0.25, whereas other outlets are dominated by river runoff (Zhang et al., 2010). Morphologically, LE can be roughly divided into three shoals (western, middle, and eastern) and two channels (eastern and western) (Fig. 1). In the along-bay direction, LE is divided into two parts by Qi'ao Island and Inner-Lingding Island (ILI), i.e., Inner-Lingding Estuary (ILE) and Outer-Lingding Estuary (OLE) (Fig. 1). The salinity of the ILE is generally low, and the strong runoff from the outlet during the flood season pushes the monthly zero iso-salt line to the outside of the ILI, while low-salinity water appears near the outlets during the dry season (Fig. 2(d)). According to records from the Guishan Island wave station, the dominant wave directed south-easterly are the dominant waves, accounting for 29% of all waves. The mean annual wave height is 0.41 m, with an average wave period of 4.50 s (Yin et al., 2017). Owing to the presence of several islands in the OLE, the wave action in the ILE is weak. In addition, the upstream runoff and sediment conditions in July 1978 and July 1999 were the normal flood season conditions in the Pearl River Estuary, and LE did not experience the impact of large to extreme flood events during the study periods.

Tides in LE are of an irregular semi-diurnal/mixed type. The annual average tides in LE range spatially between ~1.0 m (around Lantau Island) and ~1.6 m (at Dahu Tide Level Station), and range temporally from ~0.7 m during neap tides to ~2 m during spring tides around Lantau Island (Chen et al., 2016). The composition of surface sediment varies spatially in LE and consists mainly of silt and clay (Yuan et al., 2019). The mean grain diameter of surface sediment in most parts is 6–8 φ in LE (Xiao, 2012), corresponding to 0.004–0.016 mm, meaning that it is classified as cohesive sediment.

The shoreline extension rate of LE is ~17 m/yr from the 1970s to the 2000s (Chu et al., 2022), and the water volume of LE decreased by ~6.15 × 10^8 m^3 during the

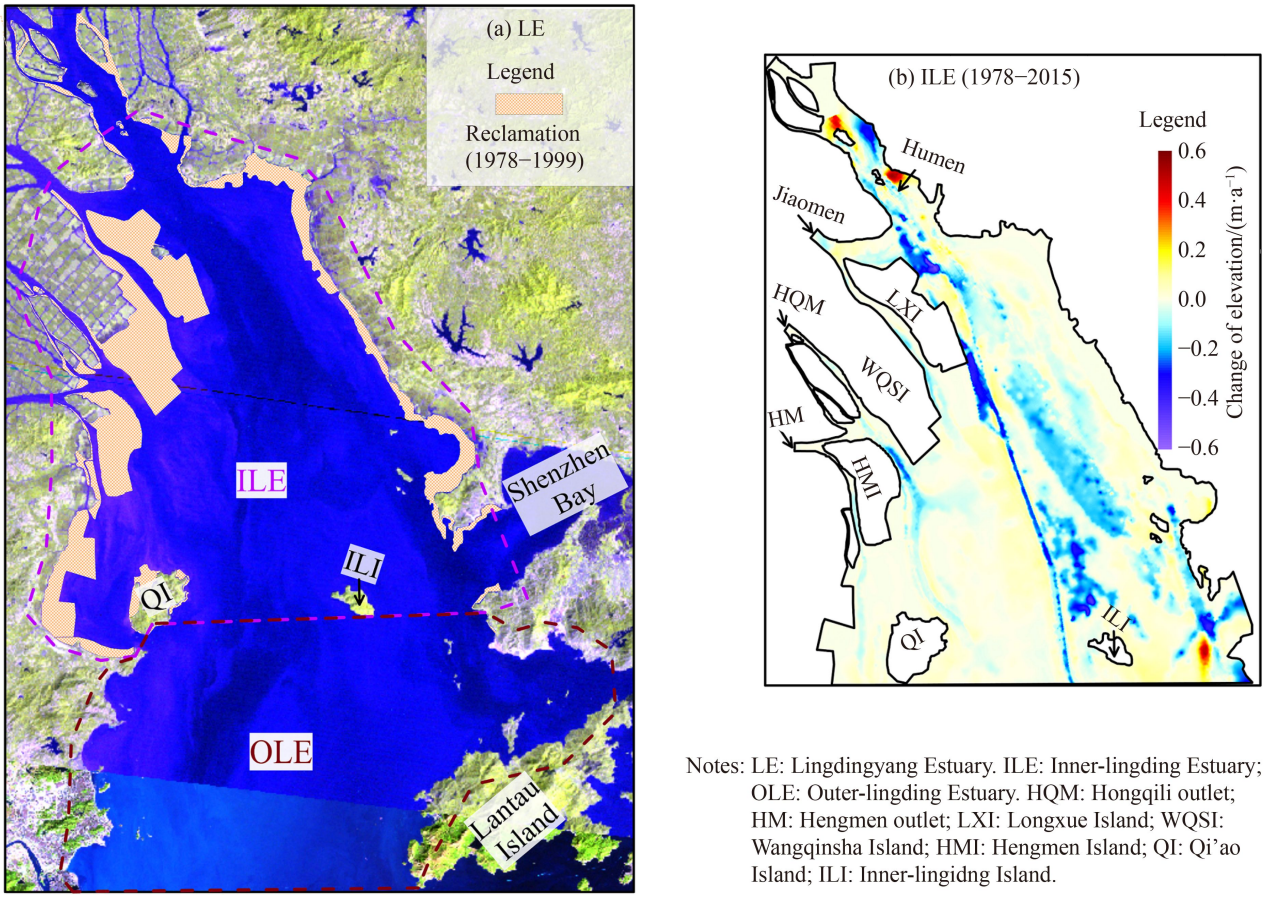

Notes: LE: Lingdingyang Estuary. ILE: Inner-lingding Estuary; OLE: Outer-lingding Estuary. HQM: Hongqili outlet; HM: Hengmen outlet; LXI: Longxue Island; WQSI: Wangqinsha Island; HMI: Hengmen Island; QI: Qi'ao Island; ILI: Inner-lingidng Island.

Fig. 1 Location of LE and variations in shoreline and bathymetry from 1978 to 2015.

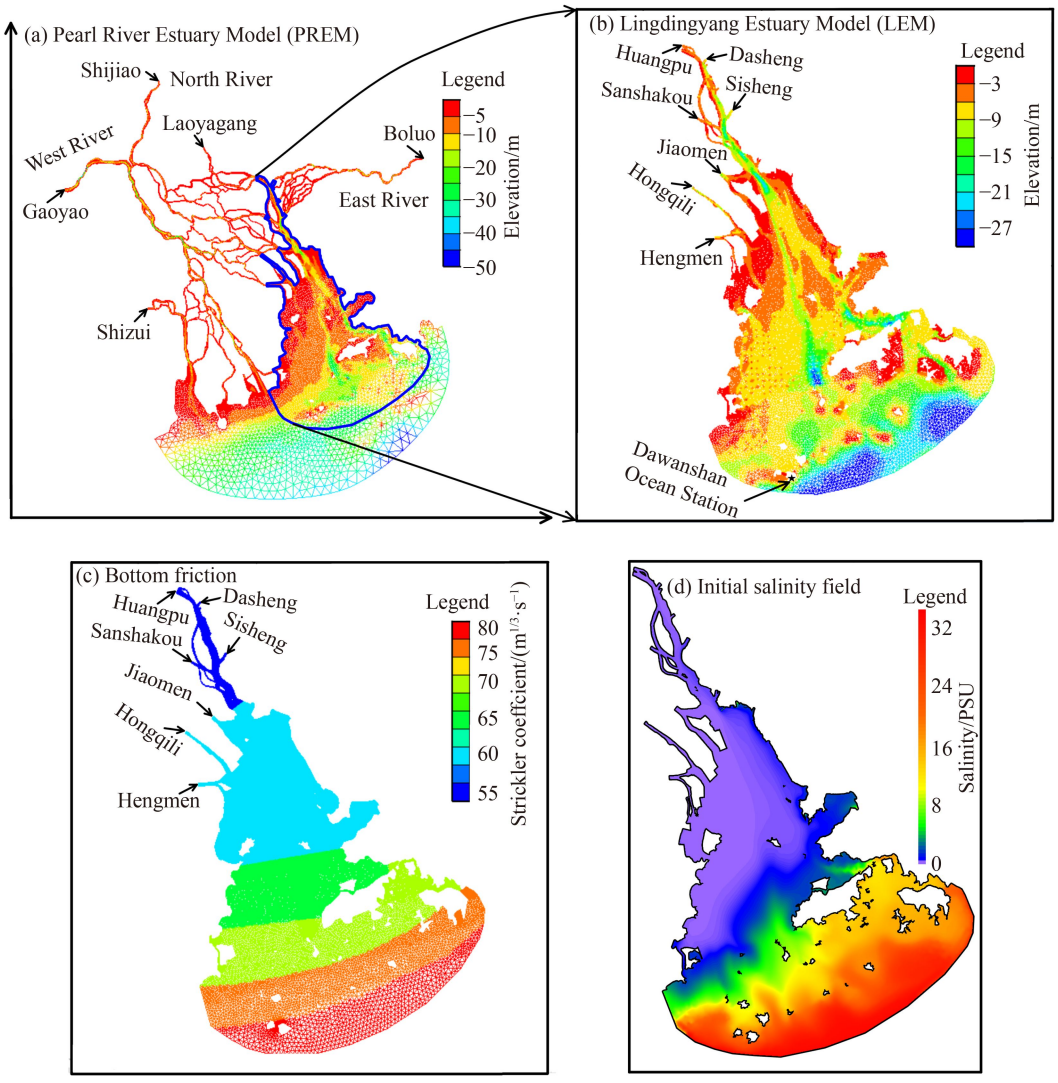

Fig. 2 Configuration of the model domain. (a) Meshes and bathymetry of the Pearl River Estuary Model (PREM). (b) Meshes and bathymetry of the Lingdingyang Estuary Model (LEM). (c) Bottom friction of the LEM. (d) Initial salinity field of the LEM given by the PREM.

period of 1955–2010 (Wu et al., 2016a). Figure 1(a) shows the reclamation of LE in the snapshots from the 1978–1999 period. In addition to reclamation, dredging is an important factor causing variations in the estuarine evolution in LE. The annual deposition rate of LE increased from 0.059 m/year during 1955–1998 to 0.081 m/year during 1998–2015, while the annual erosion rate of LE notably increased from −0.046 m/year during 1955–1998 to −0.156 m/year during 1998–2015 (Chen et al., 2020). Figure 1(b) shows the bathymetry change of LE in the snapshots from the 1978–2015 period. The past decades have witnessed continuous artificial land reclamation, which peaked from the 1970s to the 1990s, and large-scale dredging, which mainly occurred from the 2000s to the 2010s. These activities dramatically modified the boundary and morphology of LE (Figs. 1(c) and 1(d)), making it narrower and deeper.

3 Methodology

3.1 Reynolds number and Froude number

The Reynolds number (*Re*) and Froude number (*Fr*) are important dimensionless parameters that can be used to characterize the hydrodynamic characteristics of the estuarine jet flow. *Re* is a measure of the ratio of inertial to viscous forces. When fluid flows through a pipe, the fluid flow is laminar when $Re < 2300$, in a transitional state when $2300 \leqslant Re \leqslant 4000$, and turbulent when $Re > 4000$ (Pearce, 1966). *Re* is calculated as follows:

$$Re = u_0 \sqrt{h_0 b_0 / 2} / v, \tag{1}$$

where u_0 represents the average velocity at the outlet (m/s), h_0 and b_0 are the depth and width of the outlet respectively (m), and v is the kinematic viscosity, which is 10^{-6} m^2/s.

Fr is a measure of the ratio of inertial force to gravity. When $Fr < 1$, gravity plays a dominant role and the flow is slow; when $1 \leqslant Fr \leqslant 16.1$, the effect of buoyancy cannot be ignored and the estuarine jet flow is of the buoyant jet type; and when $Fr > 16.1$, the influence of buoyancy can be ignored and the estuarine jet flow is of the turbulent jet type (Hayashi, 1967, 1968). Fr is calculated as follows:

$$Fr = \frac{u_0}{\sqrt{rgh'}}, \tag{2}$$

$$r = 1 - (\rho_f / \rho_s), \tag{3}$$

where u_0 represents the average velocity at the outlet (m/s), ρ_f and ρ_s represent the densities of fresh water and seawater, respectively (kg/m^3), h' represents the depth of the density interface (m), and g represents the acceleration of gravity (9.8 m/s^2).

3.2 Coefficient of dynamic asymmetry

The effective momentum of the section not only reflects the degree of dynamic work between adjacent water bodies in the process of ebb and flow, but also quantifies the intensity of jet flows in different estuaries or at different times in the same estuary. The ratio of the effective momentum between the flood and ebb tides was used to quantify the asymmetric characteristics of the jet flow in this work. It was calculated as follows (Tang et al., 2008):

$$P = \rho \sqrt{\frac{1}{t}\int_{t_1}^{t_2} ((H+\xi)Bu)^2 \mathrm{d}t}, \tag{4}$$

$$\gamma = P_{\text{flood}} / P_{\text{ebb}}, \tag{5}$$

where P represents the effective momentum of the section (kg·m/s); H represents the average water depth of the jet mouth (m); ξ represents the tidal level (m); B represents the width of the jet mouth (m); u represents the average velocity of the jet mouth section (m/s); and t, t_1, and t_2 represent the tide durations and corresponding times, respectively; ρ is 1.0×10^3 kg/m^3. γ represents the coefficient of dynamic asymmetry, P_{flood} represents the effective momentum of the section at the flood tide (kg·m/s), and P_{ebb} represents the effective momentum of the section at the ebb tide (kg·m/s).

3.3 Modeling approach

Numerical simulations were performed using the TELEMAC-MASCARET modeling system, a package that includes modules for modeling free-surface hydrodynamics, sediment transport, water quality, waves, and groundwater flows. The system was developed by the Laboratoire National d'Hydraulique et Environnement (LNHE), a research department of Électricité de France (EDF). The TELEMAC-MASCARET system is based on an unstructured grid with finite element or finite volume numerical schemes, and is suitable for estuaries with irregular and complex geometries. Hydrodynamics were computed using the TELEMAC-2D module, and sediment transport and bed evolution were calculated using the SISYPHE module. Additional details of the TELEMAC-2D model are provided in relevant studies (Chen et al., 2022; He et al., 2022).

3.3.1 Model configuration

1) Model range and offshore salinity boundary

The hydrodynamic and sediment transport model of LE (LEM) was constructed by using the TELEMAC-2D system coupled with hydrodynamic and sediment transport modules. The model grid and computational domain are presented in Fig. 2. The unstructured grids had spatial resolutions ranging from 1200 m in the offshore region to 100 m in the upper outlet area. Sisheng, Dasheng, Huangpu, Sanshakou, Nansha, Fengmamiao, and Hengmen were set as the upstream boundary in the LEM (Fig. 2(b)), with an open boundary extending approximately to the −40 m isobaths offshore. The model used the topography measured in 1978 and 1999. The Universal Transverse Mercator (UTM) coordinate system and the Pearl River datum were used for modeling, and the terrain was based on the Pearl River datum.

The Pearl River Estuary Model (PREM) has been fully verified by a large number of tidal level stations, hydrological stations and synchronous observation data of the Pearl River network (Fig. 2(a)). For additional details on the parameter setting and validation of the PREM, the reader is referred to He et al. (2017). The stable salinity field pattern of the PREM provided the initial salinity field for the LEM (Fig. 2(d)), as well as the hourly salinity of the downstream boundary input during different simulation stages.

2) Main parameter settings

The mean particle size of surficial sediments in LE varies from 1.5φ to 7.7φ, with an average of 6.5φ (Zhao, 1981; Xiao, 2012). Therefore, the sediment particle size was set as 0.03 mm in the LEM. Strickler's law was used to calculate bottom friction, and the friction coefficients for the outlets, the estuary, and the offshore sea were set as 55 m$^{1/3}$/s, 60 m$^{1/3}$/s, 65 m$^{1/3}$/s, 70 m$^{1/3}$/s, 75 m$^{1/3}$/s, and 80 m$^{1/3}$/s (Fig. 2(c)), respectively. In previous *in situ* studies, we obtained τ_{ce} (the critical erosion shear stress of the mud) values of 0.05–0.45 N/m^2 for LE using the UMCES-Gust Erosion Microcosm System (Dong et al., 2020). The Partheniades constant was 2.0×10^{-5} kg/m^2/s. Thus, the bottom sediment was divided into four layers, and τ_{ce} values for these layers were set as 0.10 N/m^2, 0.25 N/m^2, 0.38 N/m^2, and 1.05 N/m^2. Only cohesive

sediment was considered in the LEM.

Model performance was tested at different time scales. Two simulation periods were set in this study: July 1 to July 31, 1978 (31 days in total) and from July 1 to July 31, 1999 (31 days in total) (Table 1). The time steps in the TELEMAC-2D and SISYPHE modules were 30 s and 10 s, respectively, and the model parameters during both simulation periods were identical. For the downstream boundary input, the tidal level and flow velocity of the corresponding period were obtained using the TPXO tidal prediction system.

3.3.2 Model validation

1) Verification points

There were 11 verification points in 1978 and 1999, each consisting of three types of tidal level, flow velocity, and SSC. These validation points were primarily located in the inner bay and the upstream channel of LE; only the Xiangzhou station and Guishan Island were located in the outer bay (Fig. 3).

2) Validation of bed roughness coefficient

The bed roughness setting directly affects the simulation results of hydrodynamic and sediment transport models. Therefore, based on data measured at six points in 1978 and 2000 (Figs. 3(a) and 3(c)), the Chezy-Manning roughness formula was used to verify the bed roughness of the LEM. The Chezy-Manning roughness formulas are expressed as follows (Ludwick, 1975; Knight, 1981):

$$V = C \cdot (RJ)^{1/2}, \tag{6}$$

$$C = n^{-1} \cdot R^{1/6}, \tag{7}$$

$$n = V^{-1} \cdot R^{2/3} \cdot J^{1/2}, \tag{8}$$

where V and R represent the average velocity (m/s) and average water depth (m), respectively; J represents the water surface slope (‰); C represents the Chezy coefficient ($m^{1/2} \cdot s^{-1}$); and n represents Manning coefficient ($s \cdot m^{-1/3}$).

The Manning roughness coefficient of six points at the top of LE is 0.0135–0.0172 $s \cdot m^{-1/3}$, and the corresponding Strick coefficient is 58.31–74.09 $m^{1/3} \cdot s^{-1}$ (Table 2). The ILE is mainly dominated by shoals, with the area of shoals accounting for 80% of the total area in the ILE. The average water depth of the ILE ranges from −6.5 m to −5.5 m, and the corresponding Strickler coefficient is 57–61 $m^{1/3} \cdot s^{-1}$. Thus, a Strickler coefficient of 60 $m^{1/3} \cdot s^{-1}$ was used for the ILE in the hydrodynamic and sediment transport model.

3) Model validation

Simulation results for tidal level, flow velocity and depth-averaged SSC in 1978 and 1999 were compared against measured data. The Nash Sutcliffe efficiency (*NSE*) coefficient and coefficient of determination (R^2) were used to evaluate the modeling results. *NSE* values range from $-\infty$ to 1, with values closer to 1 indicating a higher model accuracy (Sun and Su, 2020). R^2 values range from 0 to 1, with high values indicating that the independent variable can explain the variance in the dependent variable to a high degree. In this work, Q_{ob}, Q_{mo}, $\overline{Q_{ob}}$, and $\overline{Q_{mo}}$ represent the observed, simulated, averaged observed, and averaged simulated values, respectively. n represents the time series, such that the equations are written as follows:

$$NSE = 1 - \frac{\sum_{i=1}^{n} (Q_{ob} - Q_{mo})^2}{\sum_{i=1}^{n} (Q_{ob} - \overline{Q_{ob}})^2}, \tag{9}$$

$$R^2 = \frac{[\sum_{i=1}^{n} (Q_{ob} - \overline{Q_{ob}})(Q_{mo} - \overline{Q_{mo}})]^2}{\sum_{i=1}^{n} (Q_{ob} - \overline{Q_{ob}})^2 \cdot \sum_{i=1}^{n} (Q_{mo} - \overline{Q_{mo}})^2}. \tag{10}$$

The difference between the simulated and observed tidal levels was small (Table 3). The $\overline{NSE}$ and $\overline{R^2}$ values for the tidal level evaluation were 0.952 and 0.957 in 1978, and those in 1999 were 0.921 and 0.939, respectively (Table 3). The *NSE* and R^2 values of the tidal level at Xiangzhou station and Guishan Island station exceeded 0.9 (Table 3), indicating that the model results in the OLE were reasonable. In general, the flow velocity evaluation in 1978 and 1999 were good, with the values of $\overline{NSE}$ and $\overline{R^2}$ exceeding 0.85. The low validation effect of SSC is a common problem in the evaluation of the hydrodynamic and sediment transport model, but the R^2 value of SSC in the LEM also exceeded 0.65 in 1999 (Table 3).

Some sites had relatively low values for model evaluation (Table 3). Therefore, the validation curves for these sites are shown in Fig. 4. Although the R^2 values of SSC at sites L1 and G1 were less than 0.5, the variation curves of SSC at sites L1 and G1 were consistent with the measured values, and the average SSC had the same order of magnitude (Figs. 4(c) and 4(d)). For example, the

Table 1 The hydrological data of seven hydrologic stations in upstream

Hydrologic station	Period	Data types
Sisheng; Dasheng; Huangpu; Sanshakou; Nansha;	1978.07.01−1978.07.31	(Tidal level; flow velocity; SSC)[1)]
Fengmamiao and Hengmen	1999.07.01−1999.07.31	(Tidal level; flow velocity; SSC)[2)]

Notes: 1) The data were selected from the hydrology survey of LE during 1978−1979; 2) The data were selected from the simultaneous hydrologic observation data of the network river in the Pearl River Delta in July 1999.

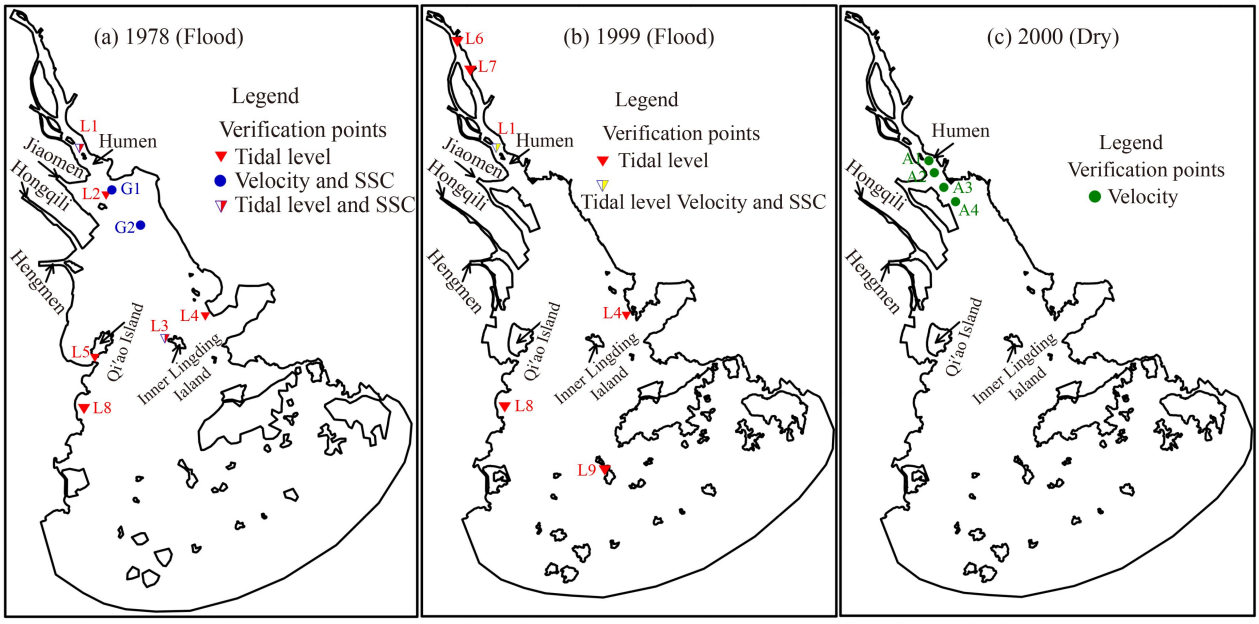

Notes: SSC: Suspended sediment concentration. L1: Dahu; L2: Shanbanzhou; L3: Inner liding; L4: Chiwan; L5: Jinxingmen; L6: Machong; L7: Zhangpeng; L8: Xiangzhou; L9: Guishan Island. The tidal level data of the Xiangzhou and Guishan Island stations were obtained from the South China Sea Bureau of the Ministry of Natural Resources.

Fig. 3 The pattern of verification points in 1978, 1999, and 2000.

Table 2 Verification of bed roughness coefficient in the LEM

Year	Verification points	R/m	V/(m·s^{-1})	J/‰	n/(s·m$^{-1/3}$)	SC/(m$^{1/3}$·s^{-1})
1978	G1	6.986	0.381	0.00282	0.0161	61.93
	G2	9.804	0.486		0.0158	63.10
2000	A1	5.823	0.241		0.0169	58.34
	A2	11.629	0.442	0.00157	0.0146	68.58
	A3	14.829	0.561		0.0135	74.09
	A4	10.327	0.377		0.0158	63.27

Notes: V and R represent average velocity and average water depth; J represents water surface slope; SC means the Strickler roughness coefficient; n means Manning coefficient. SC=1/n.

average simulated and measured SSC values at site L1 were 0.0971 kg/m^3 and 0.1017 kg/m^3, respectively. Furthermore, the daily mean sediment concentration showed a good fit with the measured data (Figs. 4(e) and 4(f)), which reproduced the variation in sediment concentrations from spring to neap tides. In general, the simulation results of the LEM in 1978 and 1999 were good, indicating that the changes in hydrodynamics and sediment transport in LE were well represented.

3.3.3 Scenarios with different influencing conditions

LE has undergone disturbance due to various anthropogenic activities over the past decades, especially extensive reclamation from the 1970s to the 1990s (Fig. 1(c)) and massive navigation channel dredging from 2000 to 2015 (Chen et al., 2020). In this study, the LEM1 and LEM2 scenarios were set based on actual conditions, and three computational scenarios of the LEM, namely LEM1-R, LEM1-D and LEM1-DR were set based on the LEM1 scenario (Table 4). LEM1-R was the scenario considering reclamation, and it used the boundary in 1999 as the model boundary to simulate the changes in hydrodynamics and sediment transport in LE in July 1978. The bathymetric setting in the LEM1-R scenario considered the reclamation area from 1978 to 1999 as land. LEM1-D was the scenario considering dredging, and it used the bathymetry of 2015 and the bathymetry of 1978 (the reclamation area from 1978 to 2015) as the model topography to simulate the changes in hydrodynamics and sediment transport in LE in July 1978. The bathymetric setting of the reclamation area from 1978 to 2015 in the LEM1-D scenario was in line with that in the LEM1 scenario to reduce the impact of hydrodynamics caused by tidal flats. LEM1-DR was the scenario considering both reclamation and dredging, and it used the boundary in 1999 as the model boundary and the bathymetry of 2015 as the model topography to

Table 3 Evaluation parameters for model at each observation site in 1978 and 1999

Sites	1978							1999						
	Tidal level		Flow velocity		SSC			Tidal level		Flow velocity		SSC		
	NSE	R^2	*NSE*	R^2	Ob	Mo	R^2	*NSE*	R^2	*NSE*	R^2	Ob	Mo	R^2
L1	0.972	0.974	–	–	0.102	0.097	0.283	0.943	0.948	0.871	0.904	0.065	0.063	0.676
L2	0.970	0.971	–	–	–	–	–	–	–	–	–	–	–	–
L3	0.932	0.938	–	–	0.120	0.115	0.680	–	–	–	–	–	–	–
L4	0.950	0.952	–	–	–	–	–	0.935	0.953	–	–	–	–	–
L5	0.938	0.950	–	–	–	–	–	–	–	–	–	–	–	–
L6	–	–	–	–	–	–	–	0.905	0.940	–	–	–	–	–
L7	–	–	–	–	–	–	–	0.900	0.913	–	–	–	–	–
L8	0.914	0.927						0.907	0.921					
L9								0.902	0.915					
G1	–	–	0.896	0.923	0.117	0.104	0.445	–	–	–	–	–	–	–
G2	–	–	0.804	0.891	0.074	0.084	0.489	–	–	–	–	–	–	–
AV	0.946	0.952	0.850	0.907	0.957	0.100	0.474	0.915	0.931	0.871	0.904	0.065	0.063	0.676

Notes: Ob: Observation value; Mo: Model value. AV: Average value. – indicates no data.

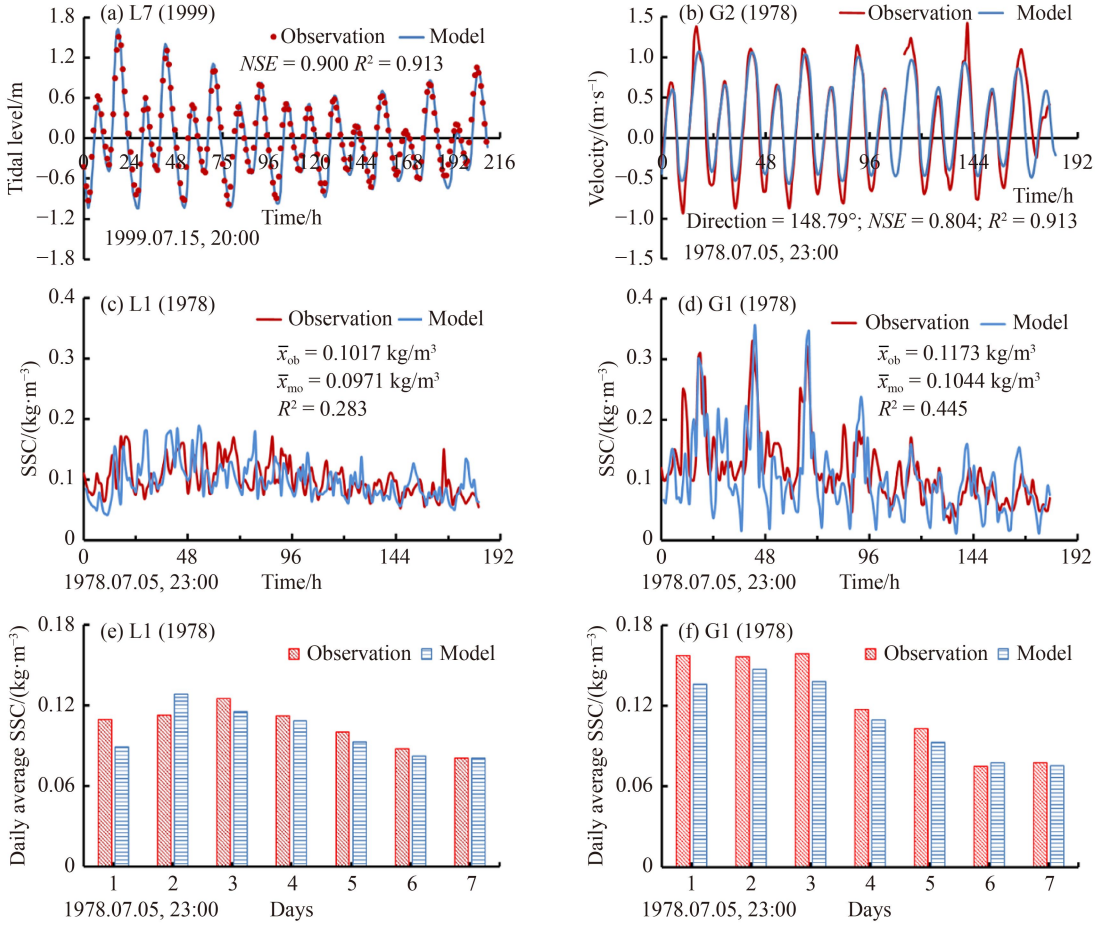

Fig. 4 Evaluation parameters for four stations of LE in 1978 and 1999.

simulate the changes in hydrodynamics and sediment transport in LE in July 1978.

Previous studies have shown that the Manning roughness coefficient varies with water depth (Ree and

Palmer, 1949). Chien et al. (1959) and Chow (1959) reported that the Manning roughness coefficient decreased with increasing water depth. Cheng et al. (1993) found that the simulation results fit well with the measured values when setting the Manning roughness coefficient in a partition. To better reflect the effect of large-scale channel dredging on the hydrodynamic and sediment transport pattern, the Manning roughness coefficients of the major channels in LEM were set by zoning in various scenarios. The Strickler coefficient of the Eastern Channel was 60 $m^{1/3}\cdot s^{-1}$ in the LEM1, LEM2, and LEM1-R scenarios, whereas it was 70 $m^{1/3}\cdot s^{-1}$ in the LEM1-D and LEM1-DR scenarios (Table 5). Similarly, the Strickler coefficient of the Western Channel was 65 $m^{1/3}\cdot s^{-1}$ in the LEM1, LEM2, and LEM1-R scenarios, whereas it was 80 $m^{1/3}\cdot s^{-1}$ in the LEM1-D and LEM1-DR scenarios. Other than the conditions specific to each scenario, all conditions of the three computational models were in line with those of the LEM1 scenario.

4 Results

4.1 Variation in dynamic pattern

4.1.1 Change in the confluence hydrodynamic zone

Channel confluences are zones with significant hydraulic and morphological variations in a fluvial-estuarine system, with extensive effects on geomorphology and ecology (Rhoads et al., 2009). As the flows from two tributaries merge and adjust to the confluence's planform geometry, considerable alterations to the flow hydrodynamics and bed morphology take place within and immediately downstream of the confluence (Yuan et al., 2018; Li et al., 2022). Within a confluence, the region where the local hydrodynamics are influenced by the convergence and realignment of the combining flows is known as the confluence hydrodynamic zone (CHZ) (Best, 1988; Kenworthy and Rhoads, 1995).

The positions of the CHZs in LE changed significantly as a result of reclamation and dredging (Fig. 5). The major differences between the CHZs in the LEM1 and LEM2 scenarios were as follows. i) Due to the reclamation of Longxue Island, the pattern of confluence of the Jiaomen and Western Channel residual currents changed from a scattered CHZ (zone A1) to two concentrated CHZs (zones B1 and B2). The location of the CHZ shifted approximately 5.2 km south-east from zone A1 to zone B2 (Fig. 5(b)). ii) After the confluence of the Hongqili and Hengmen residual currents, the CHZ in the northern branch of Hengmen Eastern Channel shifted from zone A2 to zone B3, and moved 2.8 km south-east. iii) The CHZ in the southern branch of Hengmen Eastern Channel shifted from zone A3 to zone B4, and moved 4 km south-east (Fig. 5(b)). In general,

Table 4 Scenarios of different influence conditions in LEM

Scenarios	Boundary	Bathymetry	Flow and SSC input in upstream	Tidal level and velocity in downstream
LEM1	1978	1978	In July 1978	In July 1978
LEM2	1999	1999	In July 1999	In July 1999
LEM1-R	1999	1978	In July 1978	In July 1978
LEM1-D	1978	2015*	In July 1978	In July 1978
LEM1-DR	1999	2015	In July 1978	In July 1978

Note: LEM1 is the baseline scenario for comparative analysis; except for the consideration factor of different scenarios, the other conditions of the model were consistent. *The bathymetry of the LEM1-D scenario is composed of the bathymetry in 2015 and the bathymetry in 1978 (the reclamation area from 1978 to 2015).

Table 5 The setting of Manning roughness coefficients at major channels in various scenarios

Channels	Scenarios	Water depth/m	$n/(s\cdot m^{-1/3})$	$SC/(m^{1/3}\cdot s^{-1})$
	LEM1	−8.5	0.0167	60
	LEM2	−9.0	0.0167	60
Easternchannel	LEM1-R	−8.5	0.0167	60
	LEM1-D	−12.0	0.0143	70
	LEM1-DR	−12.0	0.0143	70
	LEM1	−10.0	0.0154	65
	LEM2	−10.5	0.0154	65
Western channel	LEM1-R	−10.0	0.0154	65
	LEM1-D	−15.0	0.0125	80
	LEM1-DR	−15.0	0.0125	80

the CHZ in LE became more concentrated and shifted seaward.

Compared with LEM1, the major variations in the CHZ under the influence of different scenarios were as follows. i) In the LEM1-D scenario, most of the CHZs were changed into local circulation (Fig. 5(c)). ii) In the LEM1-R scenario, the CHZ distribution pattern was similar to that in the LEM2 scenario (Figs. 5(b) and 5(d)). iii) In the LEM1-DR scenario, the CHZ of the Humen and Jiaomen outlets was converted into local circulation, and local circulation was observed on the north-west side of ILI. In addition, the CHZ of A2 moved 3.12 km south-east to the CHZ of E3, and two small CHZs (zones A3 and A4) developed into one large CHZ (E4) (Fig. 5(e)). This indicated that reclamation was the main factor driving the southward shift of the CHZ, whereas dredging caused the CHZ to change to local circulation in LE.

4.1.2 Variation in the residual flow field

The main characteristics of the residual flow field in the LEM1 scenario were as follows (Fig. 6(a)). i) The areas of high residual flow (> 0.6 m/s) were mainly distributed at the Jiaomen and Hongqili outlets. ii) The average residual flow in the channels in LE was ~0.23 m/s, which was 1.9 times that in the shoals. iii) In general, the average residual flow in LE was directed southward, indicating that downstream runoff was one of its major driving forces.

Compared with LEM1, the major variations in the residual flow field in the LEM1-R scenario were as follows (Fig. 6(b)). i) The average residual flow in

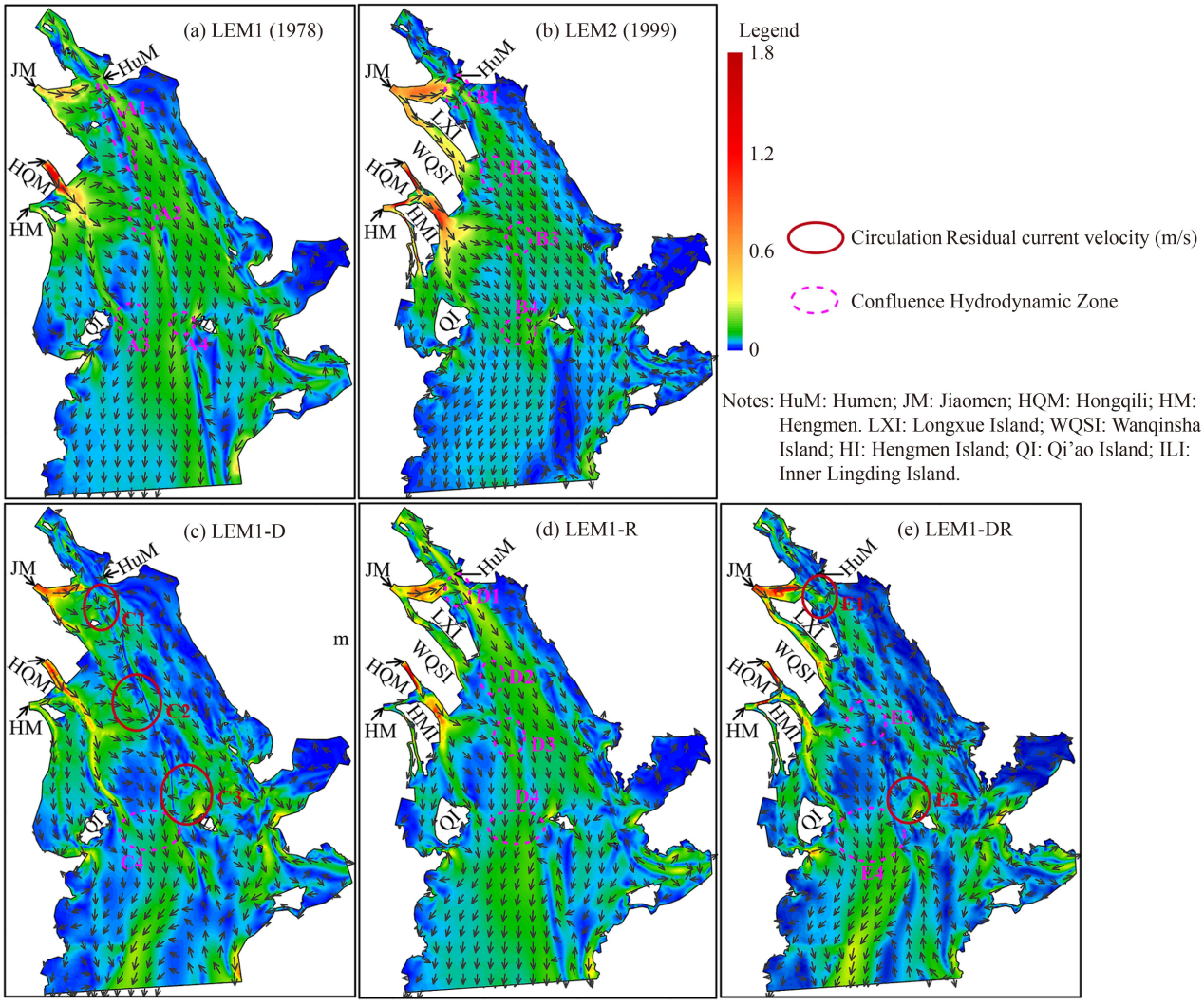

Fig. 5 Variation in the confluence hydrodynamic zone under the influence of different scenarios. The legend shows the residual current velocity (m/s). The arrows indicate only the direction of residual current, and the colors indicate the strength of residual current. The circles enclosed by purple dotted lines indicate the confluence hydrodynamic zones and the circles enclosed by red solid lines indicate the local circulation. (a) Actual condition in July 1978. (b) Actual condition in July 1999. (c) Dredging effect. (d) Reclamation effect. (e) Combined effect of reclamation and dredging.

Fuzhou Channel, Longxue South Channel, Hengmen Eastern Channel and Jinxingmen increased significantly by 0.18 m/s, 0.11 m/s, 0.16 m/s and 0.13 m/s, respectively. ii) The average residual flow in the Middle Shoal and Western Shoal in the ILE decreased slightly, by 0.04 m/s and 0.06 m/s, respectively, while those in the Middle Shoal and Western Shoal in the OLE increased slightly, by 0.05 m/s and 0.04 m/s. iii) The average residual flow outside the Longxue South "artificial outlet" and in the transition zones between the shoals and channels of LE decreased slightly, by 0.05 m/s and 0.03 m/s, respectively.

Compared with LEM1, the major changes in the residual flow field in the LEM1-D scenario were as follows (Fig. 6(c)). i) In general, the average residual flow in the channels (i.e., Chuanbi Channel and Eastern Channel) showed an obvious decrease, while that in the shoals increased. ii) The average residual flow in the Jiaomen outlet and in the southern part of the Western Shoal increased significantly, by 0.23 m/s and 0.14 m/s (Fig. 6(c)), respectively. iii) The average residual flow on the north-eastern side of Qi'ao Island increased by 0.13 m/s.

Compared with LEM1, the main variations in the residual flow field in the LEM1-DR scenario were as follows (Fig. 6(d)). i) In general, the average residual flow in the outlets and the OLE increased, whereas that in the central part of the estuary decreased. ii) In the central part of the estuary, the average residual flow in the shoals increased slightly, whereas that in the channels decreased (Fig. 6(d)). iii) In local areas, the average residual flow in the channels within the Hengmen East Channel "artificial outlet" was weakened, while that of shoals outside this outlet was strengthened.

The major variations in residual flow in different scenarios were as follows (Table 6). i) Overall, under the

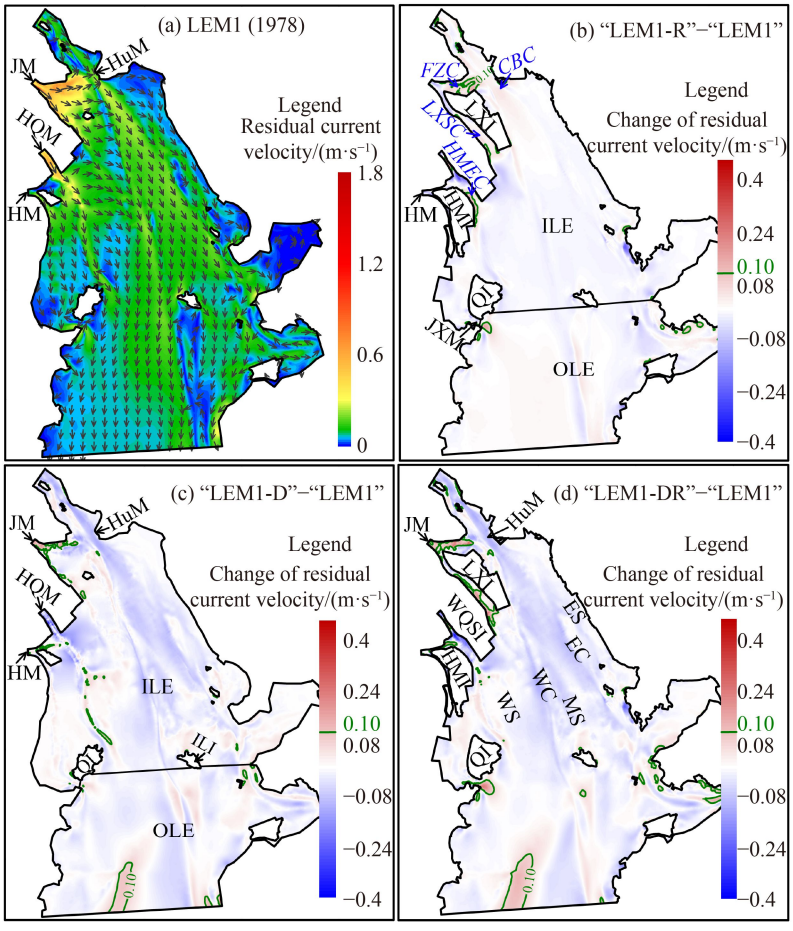

Notes: HuM: Humen; JM: Jiaomen; HQM: Hongqili; HM: Hengmen. LXI: Longxue Island; WQSI: Wanqinsha Island; HI: Hengmen Island; QI: Qi'ao Island; ILI: Inner Lingding Island.JXM: Jinxingmen. CBC: Chuanbi Channel; FZC: Fuzhou Channel; LXSC: Longxue south Channel; HMEC: Hengmen east Channel. ES: Eastern Shoal; EC: Eastern Channel; MS: Middle Shoal; WC: Western Channel; WS: Western Shoal. ILE: Inner-Lingding Estuary; OLE: Outer-Lingding Estuary.

Fig. 6 Change in residual current velocity under the influence of different scenarios. The legend of (a) shows the residual current velocity (m/s) in 1978, and the legend of (b–d) shows the change of residual current velocity (m/s). (b) Reclamation effect. (c) Dredging effect. (d) Combined effect of reclamation and dredging.

influence of reclamation only, the area of RR in the ILE accounted for ~70%, whereas that of ER in the OLE accounted for ~64%. However, the net average residual flow in LE still decreased, with the decrease being 0.0093 m/s in the ILE. ii) Overall, under the influence of dredging only, the area of ER in LE still accounted for ~65%. The net average residual flow in the ILE decreased significantly, by 0.0331 m/s, and that in the OLE decreased slightly, by 0.0046 m/s. iii) Overall, under the combined effect of reclamation and dredging, the average residual flow of LE was weakened. The area of RR in the ILE and OLE accounted for 72.10% and 56.54%, respectively. The net average residual flow in the ILE and OLE decreased by 0.0530 m/s and 0.0037 m/s, respectively.

The preceding analysis revealed that large-scale channel dredging was the major factor causing the reduction of the residual flow in LE. The rate of contribution of dredging to residual flow weakening in the ILE was 62.45%. In contrast, high-intensity reclamation weakened the residual flow in the ILE and increased that in the OLE. The contribution rate of reclamation to residual flow weakening in the ILE was 17.55%.

4.2 Variation in estuarine jet flow

Estuarine jet flow from the outlets was found to spread, with the velocity decreasing longitudinally and laterally, such that the sediment carrying capacity reduced as the area broadened (Bates, 1953; Coleman and Wright, 1975; Wu et al., 2006). The boundary of LE changed considerably from 1978 to 1999, resulting in significant variation in the estuarine jet flow pattern at the outlets (Fig. 7). i) Owing to reclamation of Longxue Island, the original estuarine jet flow at Jiaomen disappeared, and the runoff from Jiaomen bifurcated into Fuzhou Channel and Longxue South Channel. Fuzhou Channel and Chuanbi Channel converged on the north-east side of Longxue Island, forming a strong runoff interaction zone (Fig. 7(a)). ii) High-intensity reclamation of the Western Shoal in LE led to the formation of three "artificial" outlets, namely the Longxue South, Hengmen Eastern, and Hengmen Western "artificial" outlets, the locations of these outlets shifted significantly seaward, by ~13 km, ~5.7 km, and 6.5 km, respectively. iii)The structure of the bi-directional jet flow at the Humen outlet was considerably altered as a result of intensive shoreline reclamation (Fig. 7(b)). For example, the average widening rate upstream of the Humen outlet decreased notably (by ~60%) from ~0.092 in 1978 to ~0.037 in 1999, whereas that downstream of the Humen outlet decreased by 38% during the same period. In addition, the average bathymetric depth of the Humen outlet increased from −6.89 m in 1978 to −8.35 m in 1999.

4.2.1 Types of jet flow at outlets

The main characteristics of *Re* at the outlets in LE were as follows (Table 7). i) In general, the *Re* of all the outlets were in the range of 0.85~9.64 × 10^7, which were much higher than 4000. ii) The *Re* of the Humen outlet was ~9 × 10^7, which was one order of magnitude larger than that at the Hengmen Western "artificial" outlet. The *Re* of the Humen outlet at the flood tide was slightly larger than that at the ebb tide. iii) In general, the *Re* in the LEM1-R scenario was slightly smaller than that in LEM1, while that in the LEM1-D scenario was slightly larger than that in LEM1.

In situ salinity data of LE from January 14 to 22, 2000 revealed that the salinity difference between surface and bottom layers at the Humen outlet during a tidal cycle was ~10 PSU, while that at all other outlets was less than 0.5 PSU. Therefore, we concluded that the difference in water density was very small and that the *Fr* tended to infinity at all outlets, except for the Humen outlet. For the Humen outlet, we chose the salinities of 5 PSU and 20 PSU for the representative surface and bottom layers, respectively. The representative velocity and water depth were 1.0 m/s and 15 m, respectively. Thus, according to Eq. (2) and Eq. (3), the *Fr* at the Humen outlet was calculated as 158.98, which was much higher than 16.1. The flow was highly turbulent, indicating that the estuarine jet flow at the Humen outlet was a turbulent jet flow during the dry season.

Table 6 Variation of residual flow under the impact of different scenarios

Scenarios		Percent of area/%		Change of average residual flow/(m·s^{-1})		
		ER	RR	ER	RR	Net
"LEM1-R"−"LEM1"	ILE	29.90	70.10	0.050	−0.044	−0.0093
	OLE	64.30	35.70	0.021	−0.020	0.0004
"LEM1-D"−"LEM1"	ILE	35.35	64.65	0.047	−0.062	−0.0331
	OLE	34.83	65.17	0.023	−0.033	−0.0046
"LEM1-DR"−"LEM1"	ILE	27.90	72.10	0.034	−0.070	−0.0530
	OLE	43.46	56.54	0.028	−0.033	−0.0037

Notes: ER: Enhancement of residual flow; RR: Reduction of residual flow.

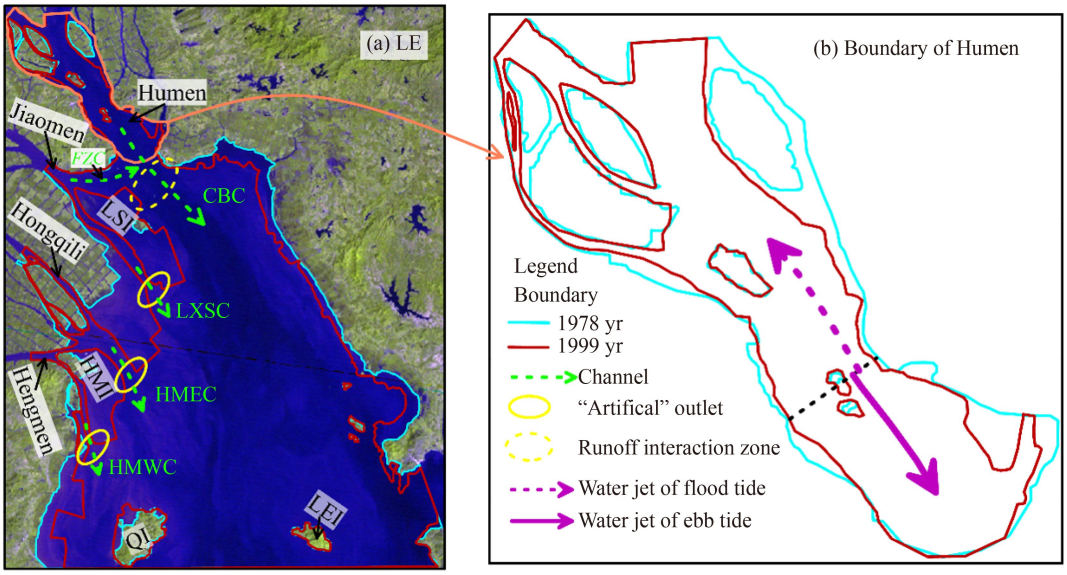

Notes: LSI: Longxue Island; HMI: Hengmen Island; QI: Qi'ao Island; ILI: Inner-lingding Island. CBC: Chuanbi Channel; FZC: Fuzhou Channel; LXSC: Longxue south Channel; HMEC: Hengmen east Channel; HMWC: Hengmen west Channel.

Fig. 7 Change in boundary in LE from 1978 to 1999.

Table 7 The Re of the outlets in LE under the impact of different scenarios ($\times 10^7$)

Scenarios	Humen		Jiaomen	Hongqili	Hengmen	LXS	HME	HMW
	Flood	Ebb						
LEM1	8.83	8.39	4.32	3.63	2.04	–	–	–
LEM1-R	8.58	8.31	–	–	–	1.31	4.07	0.85
LEM1-D	9.64	8.96	4.83	3.66	2.26	–	–	–
LEM1-DR	8.72	9.45	–	–	–	1.46	4.37	0.91

Notes: LXS: Longxue Southern "artifical" outlet; HME: Hengmen Eastern "artifical" outlet; HMW: Hengmen Western "artifical" outlet. "–" mean no data.

The aforementioned analysis of *Re* and *Fr* revealed that the estuarine jet flow at four eastern outlets and the "artificial" outlets were turbulent jet flows, and that inertial force played a dominant role.

4.2.2 Asymmetry of estuarine jet flow

The main characteristics of dynamic asymmetry at the outlets in LE were as follows (Table 8). i) Dredging had a considerable impact on the dynamic asymmetry at the Humen outlet, and the coefficient of dynamic asymmetry decreased from 0.9590 in the LEM1 scenario to 0.8607 in the LEM1-D scenario. ii) In contrast, the dynamic asymmetry at the Jiaomen outlet was greatly influenced by high-intensity reclamation; the coefficient of dynamic asymmetry decreased from 0.4313 in the LEM1 scenario to 0.3009 in LEM1-R. iii) Both reclamation and dredging resulted in the increase of the dynamic asymmetry coefficient at the Hongqili and Hengmen outlets. iv) The influence of dredging on the dynamic asymmetry at the "artificial outlets" was also obvious; for example, the coefficients of dynamic asymmetry at the Longxue South and Hengmen Western "artificial outlets" increased by ~0.042 and ~0.154, respectively.

4.3 Change in the SSC field

The pattern of SSC differed notably under the influence of reclamation and dredging (Figs. 8(a)−8(d)). In the LEM1 scenario, a high-SSC area was detected at the Jiaomen and Hongqili outlets with the average SSC > 0.2 kg/m^3. The 0.1 kg/m^3 SSC isoline was mainly observed in Eastern Channel and the central part of LE (Fig. 8(a)). In contrast with the pattern of SSC in the LEM1 scenario, i) the 0.1 kg/m^3 SSC isoline in the LEM1-R scenario was mainly located in Chuanbi Channel, Western Channel and Hengmen Eastern Channel (Fig. 8(b)); ii) the 0.1 kg/m^3 SSC isoline in the LEM1-D scenario was mainly distributed near the outlets and in the central part of LE, and the distribution area was larger than that in the LEM1 scenario (Fig. 8(c)); iii) the distribution of the 0.1 kg/m^3 SSC isoline in the LEM1-DR scenario was similar to that in the LEM1-D scenario, but the distribution range was greater than that in the

Table 8 The coefficient of dynamic asymmetry at the outlets under the impact of different scenarios

Scenarios	Humen	Jiaomen	Hongqili	Hengmen	Longxue south outlet	Hengmen east outlet	Hengmen west outlet
LEM1	0.9590	0.4313	0.5696	0.6783	–	–	–
LEM1-R	0.9587	0.3009	0.6285	0.6937	0.7098	0.8478	0.6329
LEM1-D	0.8607	0.4472	0.6104	0.6791	–	–	–
LEM1-DR	0.9154	0.2794	0.6114	0.6880	0.7515	0.8504	0.7874

Note: "–" mean no data.

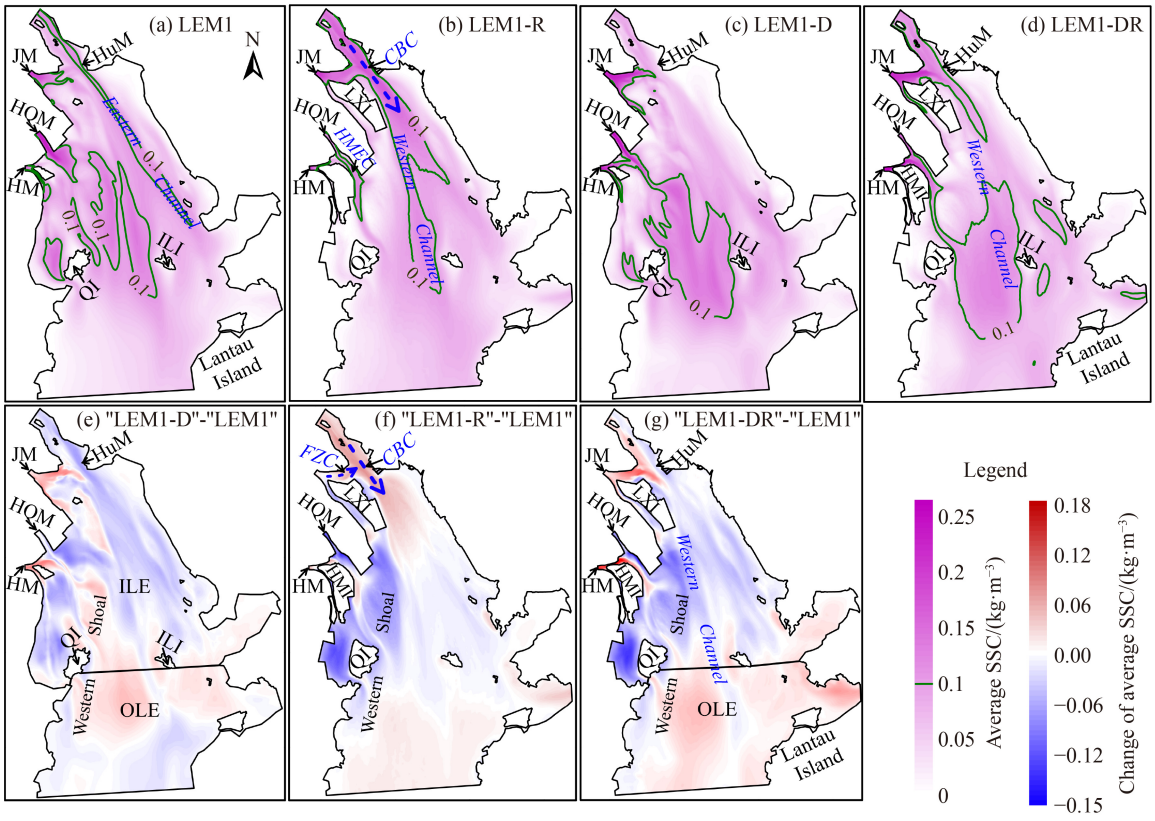

Note: HuM: Humen; JM: Jiaomen; HQM: Honqili; HM: Hengmen. LXI: Longxue Island; WQSl: Wanqinsha Island; QI: Qi'ao Island; HI: Hengmen Island; ILI: Inner-Lingding Island. ILE: Inner-Lingding Estuary; OLE: Outer-Lingding Estuary; FZC: Fuzhou Channel; CBC: Chuanbi Channel; HEMC: Hengmen Eastern Channel.

Fig. 8 Variation in the average SSC under the influence of different scenarios. The legend of (a–d) shows the average SSC (kg/m^3) and the legend of (e–g) shows the change in average SSC (kg/m^3). (e) Dredging effect. (f) Reclamation effect. (g) Combined effect of reclamation and dredging.

LEM1-D scenario and extended seaward (Fig. 8(d)).

Compared with LEM1, the main variations in the SSC field under the influence of different human activities were as follows (Figs. 8(e)−8(g)). i) In general, the average SSC of the central part of LE decreased significantly, whereas that near the outlets (i.e., Fuzhou Channel and Hengmen Eastern Channel) and in the OLE (i.e., the Western Shoal and southern part of the Middle Shoal) increased (Figs. 8(e)−8(g)). ii) In the channels, the average SSC of Eastern Channel and Western Channel in the LEM1-D scenario decreased (Fig. 8(e)), while that of Chuanbi Channel and Fuzhou Channel in the LEM1-R scenario increased (Fig. 8(f)), and that of Fuzhou Channel and Hengmen Eastern Channel in the LEM1-DR scenario notably increased (Fig. 8(g)). iii) In the shoals, the average SSC of the Jiaomen outlet, Hengmen outlet, and Western Shoal significantly increased (Fig. 8(e)), while that of the central part of LE in the LEM1-R scenario and LEM1-DR scenario notably decreased, especially in the Western Shoal (Figs. 8(f) and 8(g)). In addition, the overall variation pattern of average SSC in the LEM1-DR scenario was similar to that in the LEM1-D scenario, but range of average SSC values in the former scenario was larger than that in the latter scenario (Fig. 8(g)).

The major variations in the average SSC under the influence of different scenarios were as follows (Table 9): i) Under the impact of reclamation only (LEM1-R), the area of RS in ILE accounted for ~66%, whereas that of

Table 9 Variation of average SSC under the impact of different scenarios

Scenarios		Percent of area/%		Change of average SSC/(kg·m^{-3})		
		ES	RS	ES	RS	Net
"LEM1-R"−"LEM1"	ILE	34.24	65.76	0.031	−0.033	−0.0102
	OLE	79.44	20.56	0.008	−0.008	0.0033
"LEM1-D"−"LEM1"	ILE	37.63	62.37	0.025	−0.023	−0.0062
	OLE	54.57	45.43	0.013	-0.008	0.0074
"LEM1-DR"−"LEM1"	ILE	28.85	71.15	0.026	−0.029	−0.0118
	OLE	83.69	16.31	0.020	−0.010	0.0151

Notes: ES: Enhancement of SSC; RS: Reduction of SSC.

ES in the OLE accounted for ~79%. The net average SSC in the ILE decreased by 0.0012 kg/m^3, whereas that in the OLE increased by 0.0033 kg/m^3. ii) Under the impact of dredging only (LEM1-D), the area of ES in the OLE was essentially equal to that of RS. The net average SSC in the OLE increased by 0.0062 kg/m^3, while that in the ILE decreased by 0.0090 kg/m^3. iii) In general, the average SSC in the OLE was enhanced under the combined effect of both reclamation and dredging (LEM1-DR). The area of ES in the ILE and OLE accounted for 28.85% and 83.69%, respectively. The net SSC in the ILE decreased by 0.0118 kg/m^3, whereas that in the OLE increased significantly, by 0.0151 kg/m^3.

This analysis revealed that both extensive reclamation and dredging could decrease the SSC in the ILE and increase the SSC in the OLE, but their effects were different. Reclamation was the major factor causing the weakening of SSC in the ILE, with its contribution rate being 62.19%, whereas the contribution rate of reclamation to SSC enhancement in the OLE was 21.85%. In addition, dredging was an important factor causing the enhancement of SSC in the OLE, with its contribution rate being 49%.

5 Discussion

5.1 Variations in water surface slope and diversion ratio

Water surface slope and diversion ratio were important factors affecting the dynamics of average residual flow. Compared with the LEM1 scenario, the main variations in the water surface slope under the influence of extensive reclamation and channel dredging were as follows (Table 10). i) Overall, the water surface slope of channels at outlets increased in the LEM1-R scenario. For example, the water surface slope of Fuzhou Channel increased significantly, by 49.56%, while that of Eastern Channel and Western Channel decreased. ii) In general, the water surface slope of LE decreased in the LEM1-D scenario; in particular, the water surface slope of Hengmen Eastern Channel decreased by 27.12%. iii) The overall water surface slope pattern of LE in the LEM1-DR scenario was similar to that in the LEM1-R scenario, but the water surface slope of Eastern Channel decreased notably by 44.67%.

Table 10 The water surface slope of the main channels in LE (× 10^{-5})

Scenarios	CBC	FZC	HMEC	EC	WC
LEM1	0.115	1.147	1.158	0.338	0.402
LEM1-R	0.172	1.720	1.374	0.235	0.351
LEM1-D	0.116	1.159	0.844	0.245	0.372
LEM1-DR	0.150	1.496	1.237	0.187	0.307

Notes: CBC: Chuanbi Channel; FC: Fuzhou Channel; HMEC: Hengmen Eastern Channel; EC: Eastern Channel; WC: Western Channel.

Compared with the LEM1 scenario, the ratio of per unit width discharge of Fuzhou Channel in the LEM1-R scenario increased by 3.09%, from 71.29% to 74.38%, whereas that in the LEM1-D scenario decreased by 1.88% (Table 11). The variation of the per unit width diversion ratio in the LEM1-DR scenario was similar to that in the LEM1-R scenario, but the range of variation in the former scenario was slightly smaller than that in the latter scenario.

High-intensity reclamation increased the water surface slope at the outlets, which indicated that the increase in the barotropic pressure gradient was an important factor driving the enhancement of residual flow at the top of LE (Fig. 6(b)). In addition, the ratio of per unit width discharge in Fuzhou Channel increased notably owing to large-scale reclamation at Longxue Island, which was another important factor leading to the enhancement of residual flow in Fuzhou Channel.

5.2 Change in residual water level

The residual water level (i.e., average tide level) is the

Table 11 The ratio of per unit width discharge in the Fuzhou Channel and Longxue Southern Channel (%)

Scenarios	LEM1	LEM1-R	LEM1-D	LEM1-DR
FZC	71.29	74.38	69.41	72.94
LXSC	28.71	25.62	30.59	27.06

Notes: FZC: Fuzhou Channel; LXSC: Longxue Southern Channel.

result of the nonlinear interaction between runoff and tide dynamics in estuaries (Cai et al., 2018). Changes in the residual water level slope can directly reflect the variation characteristics of runoff and tide interaction in estuaries. The residual water level slope is calculated as follows:

$$S = \frac{(z_2 - z_1)}{\Delta x}, \tag{11}$$

where S represents the residual water level slope and z_1 and z_2 are the residual water levels at the downstream and upstream points, respectively. Δx represents the distance between the two sampling points.

To further analyze the impact of different human activities on the dynamic interaction between runoff and tides in LE, we selected residual water levels at sampling points along the channels near the outlets and at sampling points in Eastern Channel and Western Channel in LE (Fig. 9). The spatiotemporal variations in the residual water level slope in LE owing to various types of anthropogenic forcing were analyzed.

The major variations in the residual water level slope under the influence of different scenarios were as follows (Fig. 10). i) In general, the residual water level slope near the outlets changed dramatically, while that of Eastern Channel and Western Channel varied slightly (Figs. 10(d) and 10(e)). ii) Compared with the LEM1 scenario, the residual water level slope in the LEM1-R scenario increased significantly. For example, the residual water level slope in Fuzhou Channel increased from 1.45×10^{-5} in the LEM1 scenario to 2.17×10^{-5} in the LEM1-R scenario, representing an increase of ~50% (Fig. 10(b)). However, iii) compared with the LEM1 scenario, the residual water level slope in the LEM1-D scenario decreased notably. For example, the residual water level slope in Hengmen Eastern Channel decreased from 1.03×10^{-5} in the LEM1 scenario to 0.53×10^{-5} in the LEM1-R scenario, representing a decrease of ~48% (Fig. 10(c)).

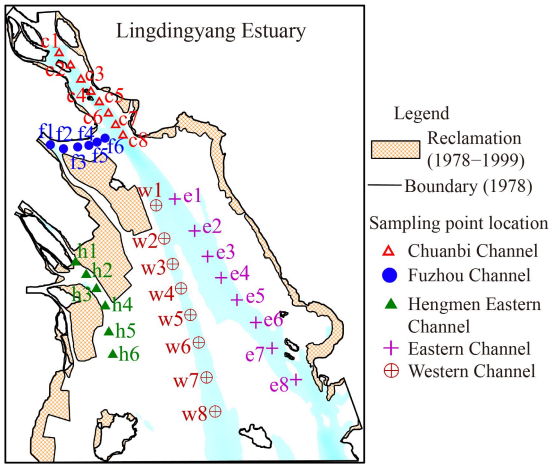

Fig. 9 The sampling points pattern of residual water level in LE.

5.3 Change in tidal wave amplitude

The tidal wave amplitude (1/2 of tidal range) is an important index for measuring the strength of tidal energy (Cai et al., 2018). To further analyze the impact of reclamation on the dynamic interaction between runoff and tides in LE, we obtained the tidal amplitudes at sampling points along the channels near the outlets and at sampling points of Eastern Channel and Western Channel in LE (Fig. 9). The spatio-temporal variations in the tidal amplitude in LE owing to various types of anthropogenic forcing were analyzed.

The main variations in the tidal wave amplitude under the influence of different scenarios were as follows (Fig. 11). i) Overall, both massive reclamation and dredging caused the increase of tidal wave amplitudes in the ILE, but the impact degree was different. ii) The average tidal wave amplitudes in Chuanbi Channel and

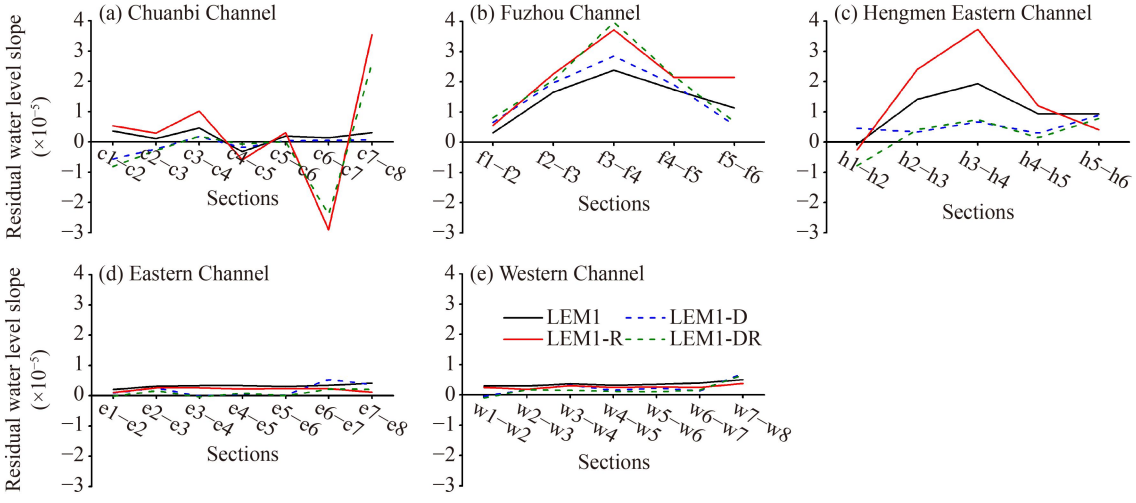

Fig. 10 The characteristics of residual water level slope in LE.

Fuzhou Channel in the LEM1-D scenario were 0.910 m and 0.809 m, which were 0.072 m and 0.063 m higher than those in the LEM1 scenario, respectively (Figs. 11(a) and 11(b)). iii) The average tidal wave amplitude in Hengmen Eastern Channel in the LEM1-DR scenario was 0.782 m, which was 0.088 m higher than that in the LEM1 scenario (Fig. 11(c)). iv) The average tidal wave amplitudes in the upstream portions of Eastern Channel (i.e., e1−e3) and Western Channel (i.e., w1−w4) in the LEM1-D scenario were 0.021 m and 0.028 m higher than those in LEM1-R scenario, respectively. In contrast, the average tidal wave amplitudes in the upstream portions of Eastern Channel (i.e., e4−e8) and Western Channel (i.e., w5−w8) in the LEM1-D scenario were 0.024 m and 0.029 m lower than those in the LEM1-R scenario (Figs. 11(d) and 11(e)), respectively.

The preceding analysis revealed that both extensive reclamation and dredging enhanced the tidal forcing in the ILE, and the enhancement of flood tide dominance was an important factor influencing the seaward weakening of the residual current in the ILE (Fig. 6). These tide regime variations were in agreement with those found in previous studies (Savenije et al., 2008; Chu et al., 2022). These variations were initiated because massive reclamation induced a convergence of tidal waves in the ILE. Chu et al. (2022) found that reclamation reduced the tidal prism of LE, which resulted in an increase in tidal energy in the ILE and a decrease in tidal energy in the OLE. In addition, dredging modified the tidal dynamics primarily through changes in bottom friction (Ralston et al., 2019). Chien et al. (1959) and Chow (1959) reported that the Manning roughness coefficient would decrease with increasing water depth. Dredging induced a decrease in bottom friction and weakened the tidal energy dissipation as the tides propagated into the ILE, causing the CHZ to change into local circulation in LE.

5.4 Comparison with the response of dynamics and sediment transport under anthropogenic activities in other estuaries

The preceding analysis shows that the hydrodynamics and sediment transport in LE have unique characteristics. First, a pattern of multiple estuarine jet flows exists in LE because of unique, narrow, rock-bound “Gates” (Wu et al., 2006); the water discharge at different outlets varies greatly, forming different estuarine jets, such as the bi-directional jet flow at the Humen outlet and the unidirectional jet flow at other outlets. Moreover, under the influence of successive episodes of land reclamation from 1978 to 1998, several new “artificial outlets” were formed and their positions moved 6–13 km seaward; the width of the northern part of the ILE also shrank by 50% (Wu et al., 2016a). In addition, under the influence of large-scale channel dredging from the 2000s to the 2010s, the depth of the Western Channel in LE increased from –10.5 m to –17.0 m and the width increased from 160 m to 240 m (Chen et al., 2020). Consequently, the hydrodynamics in LE became extremely complex. In contrast, the Yangtze Estuary is a multi-bifurcated estuary with a single input for runoff and sediment (Chen and Chen, 2007). The Yangtze Estuary is dominated by tidal currents, with the annual average ratio between runoff discharge and tidal discharge being 0.6 (Zhao et al., 2015). Owing to the influence of human activities during

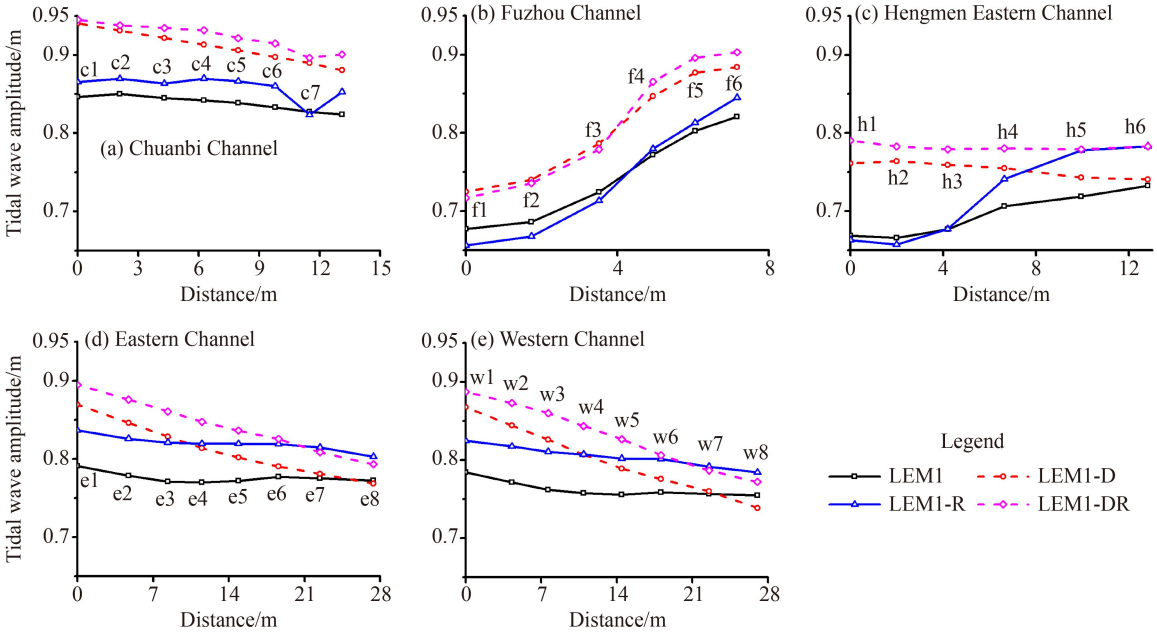

Fig. 11 Tidal wave amplitude variation of LE under the impact of different scenarios.

the past decades, the evolution of the Yangtze Estuary demonstrated a transition from natural adaptation to artificial control (Chen and Chen, 2007), with a shift in the river-tide transition in the direction of the sea (Zhang et al., 2019). As each end of South Branch in the Yangtze Estuary was restricted by reclamations, the morphology, hydrology and energy exhibited a consistent and progressive response between segments (Zhang et al., 2019). Hu and Hou (2013) reported that large scale bank protection projects controlled the basic river regime in the Yangtze Estuary. In addition, Ta et al. (2002) reported that the Mekong River Delta has been altered from a tide-dominated to a tide-wave-dominated area due to reclamation-induced tidal flat loss.

Secondly, the variation in the SSC pattern in the northern part of the ILE significantly increased owing to reclamation-induced residual flow enhancement, whereas that of the OLE increased owing to the dredging-induced residual flow enhancement, with the contribution rate being 49%. In our study, the average residual flow of the outlets was found to increase considerably, by 0.11–0.18 m/s (Fig. 6(b)), owing to the reclamation-induced increase in the residual water level slope near the outlets (Figs. 10(a)−10(c)) and the increase in the ratio of the per unit width discharge in Fuzhou Channel (Table 9). Liu et al. (2020) reported that reclamation-induced residual flow near the reclamation project increased by 0.02–0.25 m/s in LE. Moreover, several studies have reported that high-intensity reclamation can increase tidal wave deformation (Gao et al., 2014), change the plume and sediment transport (Choi, 2014), and lead to an increase in estuarine turbidity (Winterwerp et al., 2013). Cheng et al. (2020) pointed out that reclamation led to the enhancement of tidal current and the increase in SSC in Yalu River Estuary. Maren et al. (2016) pointed out that shoreline reclamation was an important factor driving the significant increase in SSC in the Ems Estuary at the Dutch-German border.

Thirdly, the reclamation-induced increase in the barotropic pressure gradient was the main factor affecting the hydrodynamics and SSC pattern near the outlets. The barotropic pressure gradient in Fuzhou Channel was always oriented eastward, and its water surface slope was one order of magnitude larger than that in Chuanbi Channel (Table 10). Moreover, the ratio of per unit width discharge in Fuzhou Channel increased by 3.09% (Table 11). Owing to these reasons, the flow rate in Fuzhou Channel was higher than the jet flow rate at the Humen outlet. Furthermore, the accumulative effect and reclamation in the key area around Longxue Island amplified the imbalance between the eastern and western parts of LE and initiated a shift in the tidal regime (Chu et al., 2022). The reclamation in the north-west portion of the inner LE resulted in more concentrated tidal energy when the tides propagated northward (e.g., increased tidal wave amplitude by ~0.04 m in Eastern Channel and Western Channel). Similar tidal variations imposed by land reclamation in the Qiantang Estuary and Hangzhou Bay system were reported by Xie et al. (2017) and Xie (2018). In addition, some previous studies stressed the importance of the bathymetric changes on estuarine hydrodynamics (Xie and Wang, 2021; Xie et al., 2022). For instance, tidal range could be doubled if the inner estuary underwent erosion. The dredging-induced decrease in the bottom friction was another major factor influencing the enhancement in tidal energy in LE when the tides propagated upward (e.g., increased tidal wave amplitude by ~0.07 m in Chuanbi Channel). In general, successive land reclamation and large-scale channel dredging during the past decades increased the relative tidal forcing in the ILE (Fig. 11), which meant stronger saltwater intrusion and higher risk of flooding. Similarly, extensive anthropogenic disturbances have strongly affected the water level variability in the Mississippi River Delta (Hiatt et al., 2019) and other deltas worldwide (Zhang et al., 2022).

Finally, due to variations in the hydrodynamics and SSC pattern, the morphologic equilibrium of submerged deltas (e.g., depocenter distribution) and water quality (e.g., saline water intrusion) may be altered (Hu et al., 2015). As reported by Tornqvist et al. (2006), the Mississippi River estuary experienced a retreat of the old subaqueous delta due to the abandonment of the old channel after channel switching, whereas a new delta and new dynamic equilibrium were formed at the location of the channel. Similar reclamation-induced sedimentation has been reported in the Yangtze Estuary (Wei et al., 2017). In addition, the narrowing of waterways due to reclamation (Chen and Zhu, 2014) and the increase in bathymetric depth due to dredging (Wu et al., 2016b) has led an increase in salinity in the Yangtze Estuary. Shen et al. (2018) pointed out that reclamation impeded runoff and resulted in an increase in salinity in the Pearl River Estuary. A similar geomorphological pattern and saltwater intrusion may also occur in LE. However, since LE is a wide estuarine bay system, the magnitude of the system's response to the multiple types of anthropogenic forcing is unclear. Thus, the depocenter transfer and water security warrant further study.

6 Conclusions

An internally coupled TELEMAC-2D and SISYPHE model for LE was established to explore variations in hydrodynamics and sediment transport and to analyze its response to reclamation and dredging. The main conclusions are as follows.

i) Owing to successive land reclamation, the general distribution of the CHZs in LE varied from scattered in 1978 to concentrated in 1999, and these zones moved 3–5 km seaward. In addition, dredging induced the

enhancement of flood tide dominance and caused the CHZs in LE to change into local circulation.

ii) Large-scale dredging was the major factor causing the weakening of residual flow in LE, decreasing the residual flow in the ILE by 62.45%. This was initiated by an enhancement of tidal dynamics through changes in the bottom friction caused by dredging in the ILE. In contrast, extensive land reclamation decreased the residual flow in the ILE by 17.55% and increased that in the OLE.

iii) Despite reclamation- and dredging-related disturbances, the estuarine jet flow in LE remained a turbulent jet system, and the positions of the estuarine jet sources moved 6–13 km outward. Large-scale dredging was the main factor affecting the dynamic asymmetry at Humen outlet with the γ coefficient decreasing by ~0.10. However, extensive reclamation was the major factor affecting the dynamic asymmetry at Jiaomen outlet with the γ coefficient decreasing by ~0.13. The combined effects of reclamation and dredging altered the dynamic asymmetry at the newly formed "artificial outlets."

iv) Both extensive reclamation and dredging decreased the SSC in the ILE and increased the SSC in the OLE, but the magnitude of the impact was different. Reclamation was the main factor causing the weakening of SSC (by 62.19%) in the ILE, whereas dredging was an important factor causing the enhancement of SSC in the OLE, with the contribution rate being 49%. Spatially, reclamation led to an increase in SSC near the outlets and a decrease in SSC in the northern part of the Western Shoal. Dredging mainly caused an increase in the SSC in the central portion of LE, especially in the north of the OLE.

v) As a result of intensive land reclamation, the increase in the per unit width discharge and barotropic pressure gradient were the major factors driving the enhancement of the residual flow and SSC in the Fuzhou channel. Moreover, the southward locations of the "artificial outlets" favored the transport of suspended sediments to the OLE. Finally, the general tidal dynamics in the LE were enhanced by successive land reclamation and large-scale dredging. Owing to these anthropogenic interferences, the variations in tidal dynamics notably affected the distribution of SSC in the ILE.

These findings show that the hydrodynamics and sediment transport can be notably altered by extensive reclamation and dredging. This insight is of practical significance to comprehensive management of estuaries and the formulation of major future estuarine engineering projects. Finally, the results of this study enrich our understanding of the response of hydrodynamics and SSC in LE to changes in shoreline and bathymetry, which could be of practical importance for other estuaries subjected to similar stresses.

Acknowledgments This study is funded by the National Natural Science Foundation of China (Grant Nos. 42201104, 41376101, and 42071123), China Postdoctoral Research Foundation (Grant No. 2023M730758), Guangdong Provincial Special Key Project of Six Marine Industries in 2022 "Research on Three-dimensional Efficient Utilization of Marine Spatial Resources in Guangdong-Hong Kong-Macao Greater Bay Area" ([2022]49). Thanks to the Guangdong Provincial Department of Hydrology Bureau for providing relevant data of runoff and sediment in upstream boundary input. We thank the editor and anonymous reviewers whose invaluable and constructive suggestions greatly improve the scientific quality of the original manuscript.

References

Anthony E J, Brunier G, Besset M, Goichot M, Dussouillez P, Nguyen V L (2015). Linking rapid erosion of the Mekong River delta to human activities. Sci Rep, 5(1): 14745

Bates C C (1953). Rational theory of delta formation. Bull Am Assoc Petrol Geologists, 37: 2119–2161

Best J L (1988). Sediment transport and bed morphology at river channel confluences. Sedimentology, 35(3): 481–498

Cai H Y, Yang H, Guo X J, Yang Q S, Ou S Y (2018). Investigation of temporal-spatial distribution patterns of residual water level under the influence of tide-river interaction in the Modaomen Estuary, Zhujiang River. Acta Oceanolog sin, 40(07): 55–65 (in Chinese)

Chen J Y, Chen S L (2002). Estuary and coastal challenges in China. Mar Geol Lett, 18: 1–5 (in Chinese)

Chen J Y, Chen S L (2007). Fifty years of estuarine research in China: review and prospect. Oceanol Limnol Sin, 38: 481–485 (in Chinese)

Chen J, Zhu J R (2014). Impact of the reclamation project of Xincunsha on the saltwater intrusion in the North Branch of the Changjiang Estuary. J East China Normal U (Nat Sci), (04): 163–172 (in Chinese)

Chen K L, Dong H Y, Jia L W, He Z X (2020). Depocentre transfer in the Lingdingyang estuary: interferences from natural and anthropogenic forcings. Ocean Coast Manage, 185: 1–15

Chen K L, He Z X, Liu J, Lin Y T, Jia L W (2022). Long-term morphological evolution and its mechanism of Lingdingyang Estuary: interferences from anthropogenic forcings. Mar Geol, 450: 106856

Chen Z, Pan J, Jiang Y (2016). Role of pulsed winds on detachment of low salinity water from the Pearl River Plume: upwelling and mixing processes. J Geophys Res Oceans, 121(4): 2769–2788

Cheng R T, Casulli V, Gartner J W (1993). Tidal, residual, intertidal mudflat (TRIM) model and its applications to San Francisco Bay, California. Estuar Coast Shelf Sci, 36(3): 235–280

Cheng Z X, Jalon-Rójas I, Wang X H, Liu Y (2020). Impacts of land reclamation on sediment transport and sedimentary environment in a macro-tidal estuary. Estuar Coast Shelf Sci, 242: 106861

Chien N, Hon Y C, Mac C W, Pi T F (1959). Channel roughness of lower Yellow River. J Sediment Res, 4: 1–15 (in Chinese)

Choi K (2014). Morphology, sedimentology and stratigraphy of Korean tidal flats-implications for future coastal managements. Ocean Coast Manage, 102: 437–448

Chow V T (1959). Open-Channel Hydraulics. New York: McGraw-Hill

Chu N Y, Yao P, Ou S Y, Wang H, Yang H, Yang Q S (2022). Response of tidal dynamics to successive land reclamation in the

Lingding Bay over the last century. Coast Eng, 173: 104095

Coleman J M, Wright L D (1975). Modern river deltas: variability of process and sand bodies. In: Brunssard M L, ed. Deltas: Models for Exploration. Houston Geofsociety, 91–149

Dam G, Poortman S E, Bliek A J, Plancke Y (2013). Long-term modeling of the impact of dredging strategies on morpho-and hydrodynamic developments in the western scheldt. In: Proceedings WODCON XX - Congress and Exhibition: the Art of Dredging

Dong H Y, Jia L W, He Z X, Yu M D, Shi Y H (2020). Application of parameters and paradigms of the erosion and deposition for cohesive sediment transport modelling in the Lingdingyang Estuary, China. Appl Ocean Res, 94: 101999

Gao G D, Wang X H, Bao X W (2014). Land reclamation and its impact on tidal dynamics in Jiaozhou Bay, Qingdao, China. Estuar Coast Shelf Sci, 151: 285–294

Grasso F, Le Hir P (2019). Influence of morphological changes on suspended sediment dynamics in a macrotidal estuary: diachronic analysis in the Seine Estuary (France) from 1960 to 2010. Ocean Dyn, 69(1): 83–100

Hallegatte S, Green C, Nicholls R J, Corfee-Morlot J (2013). Future flood losses in major coastal cities. Nat Clim Chang, 3(9): 802–806

Hayashi S N (1967). Diffusion of Warm Water Jets Discharge Horizontally at the Water Surface. Internat Assoc Hydraulic Research, 12th Cong Proc., 4: 47–59

Hayashi S N (1968). Diffusion of Cooling Water Discharge from a Power Plant: Conf Coastal Eng. London: Council Wave Research

He J W, Jia L W, Wei X G, Jia Y H, Cheng C (2017). The 2D distribution characteristics and formation mechanism of suspended sediment concentration during the flood season in the Lingdingyang Estuary. Acta Oceanolog sin, 39: 26–39 (in Chinese)

He Z X, Liang M E, Jia L W, Dong H Y, Chen K L, Liu J, Lin Y T, Ou J T (2022). Long-term morphological modeling and implication for estuarine regulation of the Modaomen Estuary, Pearl River Delta, China. Appl Ocean Res, 123: 103184

Hiatt M, Snedden G, Day J W, Rohli R V, Nyman J A, Lane R, Sharp L A (2019). Drivers and impacts of water level fluctuations in the Mississippi River delta: implications for delta restoration. Estuar Coast Shelf Sci, 224: 117–137

Hu C Y, Hou W G (2013). Research on river regime control of mid and lower Yangtze River. Yangtze River, 44: 10–15 (in Chinese)

Hu Z, Wang Z B, Zitman T J, Stive M J F, Bouma T J (2015). Predicting long-term and short-term tidal flat morphodynamics using a dynamic equilibrium theory. J Geophys Res Earth Surf, 120(9): 1803–1823

Kenworthy S T, Rhoads B L (1995). Hydrologic control of spatial patterns of suspended sediment concentration at a stream confluence. J Hydrol (Amst), 168(1–4): 251–263

Knight D W (1981). Some field measurements concerned with the behaviour of resistance coefficients in a tidal channel. Estuar Coast Shelf Sci, 12(3): 303–322

Li C C (2004). Process and Evolution of Estuaries in Southern China. Beijing: Science Press (in Chinese)

Li K, Tang H W, Yuan S Y, Xiao Y, Xu L, Huang S J, Rennie C D, Gualtieri C (2022). A field study of near-junction-apex flow at a large river confluence and its response to the effects of floodplain flow. J Hydrol (Amst), 610: 127983

Li T J (2017). Analysis of Lingding Bay Landform Stage Evolution and Trends. Dissertation for Doctor Degree. Wuhan: China University of Geoscience (in Chinese)

Liu J T, Hu J T, Li S Y, Xu Y J, Xu C (2020). A model study on the short-term impact of reclamation on the hydrodynamic processes in the Lingdingyang Bay. Marine Science Bulletin, 39: 178–190 (in Chinese)

Ludwick J C (1975). Variations in the boundary-drag coefficient in the tidal entrance to Chesapeake Bay, Virginia. Mar Geol, 19(1): 19–28

Maselli V, Trincardi F (2013). Man made deltas. Sci Rep, 3(1): 1926

Pearce A F (1966). Critical Reynolds number for fully-developed turbulence in circular submerged water jets. Nat Mech Eng Research Inst, Council Sci and Indus Research (Pretoria,South Africa), CSIR Rept., MEG475

Perkins M J, Ng T P T, Dudgeon D, Bonebrake T C, Leung K M Y (2015). Conserving intertidal habitats: what is the potential of ecological engineering to mitigate impacts of coastal structures. Estuar Coast Shelf Sci, 167: 504–515

Pritchard D W (1967). What is an estuary: physical viewpoint In: Lanff G H, ed. Estuaries. AAAS Pub.83, Washington, D.C., 3–5

Ralston D K, Talke S, Geyer W R, Al-zubaidi H A M, Sommerfield C K (2019). Bigger tides, less flooding: effects of dredging on barotropic dynamics in a highly modified estuary. J Geophys Res Oceans, 124(1): 196–211

Ree W O, Palmer V J (1949). Flow of water in channels protected by vegetative linings. US Dept. of Agriculture

Reid J L, Seiler L L, Siegle E (2022). The influence of dredging on estuarine hydrodynamics: historical evolution of the Santos estuarine system, Brazil. Estuar Coast Shelf Sci, 279: 108131

Rhoads B L, Riley J D, Mayer D R (2009). Response of bed morphology and bed material texture to hydrological conditions at an asymmetrical stream confluence. Geomorphology, 109(3–4): 161–173

Savenije H H G, Toffolon M, Haas J, Veling E J M (2008). Analytical description of tidal dynamics in convergent estuaries. J Geophys Res Oceans, 113(C10): 1–18

Shen Y M, Jia H, Li C P, Tang J (2018). Numerical simulation of saltwater intrusion and storm surge effects of reclamation in Pearl River Estuary, China. Appl Ocean Res, 79: 101–112

Shen Y M, Zhang H X, Tang J (2022). Hydrodynamics and water quality impacts of large-scale reclamation projects in the Pearl River Estuary. Ocean Eng, 257: 111432

Smith J E, Friedrichs C (2011). Size and settling velocities of cohesive flocs and suspended sediment aggregates in a trailing suction hopper dredge plume. Cont Shelf Res, 31(10): S50–S63

Song Z K (2013). Analysis of reclamation in the north branch and its effects on hydrodynamic environment and morphological change for nearly 30 years. Dissertation for Doctor Degree. Shanghai: East China Normal University (in Chinese)

Sun H, Su F G (2020). Evaluation of multiple precipitation datasets and their potential utilities in hydrologic modeling over the Yarlung Zangbo River Basin. Prog Geogr, 39(7): 1126–1139 (in Chinese)

Ta T K O, Nguyen V L, Tateishi M, Kobayashi I, Saito Y, Nakamura T (2002). Sediment facies and Late Holocene progradation of the

Mekong River Delta in Bentre Province, southern Vietnam: an example of evolution from a tide-dominated to a tide- and wave-dominated delta. Sediment Geol, 152(3–4): 313–325

Tang Z M, Ren J, Wu C Y (2008). Study on parameters of the gate bi-direction jet current in the Pearl River Estuary. Ludong U J (Nat Sci Ed), 24: 358–362 (in Chinese)

Törnqvist T E, Bick S J, van der Brog K, de Jong A F M (2006). How stable is the Mississippi delta? Geology, 34(8): 697–700

van Maren D S, Beemster J G W, Wang Z B, Khan Z H, Schrijvershof R A, Hoitink A J F (2023). Tidal amplification and river capture in response to land reclamation in the Ganges-Brahmaputra delta. Catena, 220: 106651

van Maren D S, Oost A P, Wang Z B, Vos P C (2016). The effect of land reclamations and sediment extraction on the suspended sediment concentration in the Ems Estuary. Mar Geol, 376: 147–157

van Maren D S, van Kessel T, Cronin K, Sittoni L (2015). The impact of channel deepening and dredging on estuarine sediment concentration. Cont Shelf Res, 95: 1–14

Wang Z B, Van Maren D S, Ding P X, Yang S L, Van Prooijen B C, De Vet P L M, Winterwerp J C, De Vriend H J, Stive M J F, He Q (2015). Human impacts on morphodynamic thresholds in estuarine systems. Cont Shelf Res, 111: 174–183

Wei W, Dai Z J, Mei X F, Liu J P, Gao S, Li S S (2017). Shoal morphodynamics of the Changjiang (Yangtze) estuary: influences from river damming, estuarine hydraulic engineering and reclamation projects. Mar Geol, 386: 32–43

Winterwerp J C, Wang Z B (2013). Man-induced regime shifts in small estuaries—I: theory. Ocean Dyn, 63(11–12): 1279–1292

Winterwerp J C, Wang Z B, van Braeckel A, van Holland G, Kösters F (2013). Man-induced regime shifts in small estuaries—II: a comparison of rivers. Ocean Dyn, 63(11–12): 1293–1306

Woodruff J D, Irish J L, Camargo S J (2013). Coastal flooding by tropical cyclones and sea-level rise. Nature, 504(7478): 44–52

Wu C Y, Ren J, Bao Y, Shi H Y, Lei Y P, He Z G, Tang Z M (2006). A preliminary study on the morphodynamic evolution of the “gate” of the Pearl River delta, China. Acta Geogr Sin, 61: 537–548 (in Chinese)

Wu S H, Cheng H Q, Xu Y J, Li J F, Zheng S W (2016b). Decadal changes in bathymetry of the Yangtze River Estuary: human impacts and potential saltwater intrusion. Estuar Coast Shelf Sci, 182: 158–169

Wu Z Y, Saito Y, Zhao D N, Zhou J Q, Cao Z Y, Li S J, Shang J H, Liang Y Y (2016a). Impact of human activities on subaqueous topographic change in Lingding Bay of the Pearl River estuary, China, during 1955–2013. Sci Rep, 6(1): 37742

Xiao Z J (2012). Characteristics and transport trend of surface sediments in Pearl River Estuary and the adjacent sea area . Marine Science Bulletin, 31, 481–488 (in Chinese)

Xie D F (2018). Modeling the morphodynamic response of a large tidal channel system to the large-scale embankment in the Hangzhou Bay, China. Anthropocene Coasts, 1: 89–100

Xie D F, Pan C H, Wu X G, Gao S, Wang Z B (2017). Local human activities overwhelm decreased sediment supply from the Changjiang River: continued rapid accumulation in the Hangzhou Bay-Qiantang Estuary system. Mar Geol, 392: 66–77

Xie D F, Wang Z B (2021). Seasonal tidal dynamics in the Qiantang Estuary: the importance of morphological evolution. Front Earth Sci (Lausanne), 9: 782640

Xie D F, Wang Z B, Huang J, Zeng J (2022). River, tide and morphology interaction in a macro-tidal estuary with active morphological evolutions. Catena, 212: 106131

Yuan S, Tang H, Xiao Y, Qiu X, Xia Y (2018). Water flow and sediment transport at open-channel confluences: an experimental study. J Hydraul Res, 56(3): 333–350

Yuan X Q, Yang Q S, Luo X X, Yu F L, Liu F, Li J Y, Wang Z H (2019). Distribution of grain size and organic elemental composition of the surficial sediments in Lingding Bay in the Pearl River Delta, China: a record of recent human activity. Ocean Coast Manage, 178: 104849

Yang Y, Chui T F M (2017). Hydrodynamic and transport responses to land reclamation in different areas of semi-enclosed subtropical bay. Cont Shelf Res, 143: 54–66

Yin Y, Jiang L F, Zhang Z X, Yu H B, Wang H L (2017). Statistical analysis of wave characteristics in the Pearl River Estuary. J Tropical Oceanogr, 36: 60–66 (in Chinese)

Zhang D, Xie W M, Shen J, Guo L C, Chen Y, He Q (2022). Sediment dynamics in the mudbank of the Yangtze River Estuary under regime shift of source and sink. Int J Sediment Res, 37(1): 97–109

Zhang M, Townend I, Zhou Y X, Wang L H, Dai Z J (2019). An examination of estuary stability in response to human interventions in the South Branch of the Yangtze (Changjiang) Estuary, China. Estuar Coast Shelf Sci, 228: 106383

Zhu Q, Wang Y P, Ni W, Gao J, Li M, Yang L, Gong X, Gao S (2016). Effects of intertidal reclamation on tides and potential environmental risks: a numerical study for the southern Yellow Sea. Environ Earth Sci, 75(23): 1472

Zhao H T (1981). Bottom relief of lingdingyang in the Zhujiang River Estuary. Acta Oceanol Sin, 3: 255–274 (in Chinese)

Zhang W, Ruan X, Zheng J, Zhu Y, Wu H (2010). Long-term change in tidal dynamics and its cause in the Pearl River Delta, China. Geomorphology, 120: 209–223

Zhao D Z, Zhang J Y, Gao M (2015). Importance of the ratio between runoff discharge and tidal discharge in the regulation of multi-branch estuaries. In: Proceedings of the 17th China Ocean (Shore) Engineering Symposium, 1035–1038 (in Chinese)